2009

NANOMECHANICAL CHARACTERIZATIONS OF HIGH TEMPERATURE POLYMER MATRIX COMPOSITE RESIN: PMR-15 POLYIMIDE

David C. Jones
University of Kentucky, dcjone0@gmail.com

ABSTRACT OF THESIS

NANOMECHANICAL CHARACTERIZATIONS OF HIGH TEMPERATURE POLYMER MATRIX COMPOSITE RESIN: PMR-15 POLYIMIDE

High Temperature Polymer Matrix Composites (HTPMCs) are widely used by the aerospace industry today because of their high specific strengths, light weight, and the ability to custom tailor their mechanical properties to individual applications. Because of the harsh environmental conditions these materials experience during service use, these composite structures are susceptible to a high rate of thermo-oxidative degradation that ultimately causes premature failure in service. The current knowledge base is lacking in the fundamental spatial variability of the constituent materials upon aging, which precludes composite developers from predicting lifetime mechanical properties of the composites in use. The current study summarizes state of the art techniques in characterizing the thermally oxidized matrix resin system (PMR-15 polyimide), and develops novel techniques in direct mechanical measurement of the spatial variability of mechanical properties. Works to date and future advances in the field with respect to in situ testing are presented.

KEYWORDS: PMR-15, Nanoindentation, Oxidation, HTPMC, Polymer

David C. Jones

22 April 2009

NANOMECHANICAL CHARACTERIZATIONS OF HIGH TEMPERATURE POLYMER MATRIX COMPOSITE RESIN: PMR-15 POLYIMIDE

By

David C. Jones

Dr. Y. Charles Lu

Director of Thesis

Dr. L. Scott Stephens

Director of Graduate Studies

22 April 2009

RULES FOR THE USE OF THESES

Unpublished theses submitted for the Master's degree and deposited in the University of Kentucky Library are as a rule open for inspection, but are to be used only with due regard to the rights of the authors. Bibliographical references may be noted, but quotations or summaries of parts may be published only with the permission of the author, and with the usual scholarly acknowledgments.

Extensive copying or publication of the thesis in whole or in part also requires the consent of the Dean of the Graduate School of the University of Kentucky.

A library that borrows this thesis for use by its patrons is expected to secure the signature of each user.

Name Date

_____

_____

_____

_____

_____

_____

_____

_____

_____

_____

_____

THESIS

DAVID C. JONES

The Graduate School

University of Kentucky

2009

NANOMECHANICAL CHARACTERIZATIONS OF HIGH TEMPERATURE POLYMER MATRIX COMPOSITE RESIN: PMR-15 POLYIMIDE

THESIS

A thesis submitted in partial fulfilment of the requirements
for the degree of Master of Science in
Mechanical Engineering in the College of Engineering at the
University of Kentucky

By

David C. Jones

Lexington, Kentucky

Director:

Dr. Y. Charles Lu, Assistant Professor of Mechanical Engineering

Lexington, Kentucky

2009

I would like to dedicate this work to Tracer,

whose life inspires me to do great things.

ACKNOWLEDGEMENTS

I would like to express my deepest appreciation and respect to my academic advisor Dr. Y. Charles Lu who not only encouraged me to continue my post-baccalaureate education at the University of Kentucky, but also provided constant support through the more difficult moments of my educational and personal life.

I would like to thank Dr. Greg Schoeppner and the Air Force Research Laboratory at Wright Patterson Air Force Base, Ohio, for opening the doors to making this research possible.

I would like to thank my undergraduate research advisor, Dr. Jack Leifer, for providing me countless opportunities in the aerospace field, which brought my educational experience to higher level, as well as Dr. Karen Hackney and the late Dr. Richard Hackney of Kentucky Space Grant Consortium, whose generous financial support made this available.

Lastly, I would like to express my deepest gratitude to Dr. Tim Wu, and Dr. Christine Trinkle for accepting to be part of my thesis committee and for their valuable time in spite of their busy schedules.

TABLE OF CONTENTS

LIST OF TABLES

LIST OF FIGURES

CHAPTER ONE INTRODUCTION

1.1 BACKGROUND

Polymer matrix composites (PMCs) have been increasingly used in high temperature aerospace and space applications such as aircraft turbine engines and rocket components. The designed service life is typically 60,000 hours under sustained high temperatures. Under such conditions, the materials are subjected to thermomechanical stress, high temperature, moisture and corrosion and experience thermomechanical degradation due to thermal oxidation, which can cause premature failure of the composite structures. The failure of the composites in these aggressive environments has a direct impact on the aircraft cost and mission readiness. There is a strong need to predict the lifetime and structural durability of high temperature polymer matrix composites (HTPMCs) in structural applications.

The service-life prediction of HTPMCs based on their viscoelastic behavior has been extensively studied through the NASA High-Speed Research (HSR) program [**1**,**2**,**3**,**4**,**5**,**6**,**7**]. The elevated temperature long-term creep curves were determined using the time-temperature superposition principle, from which the "effective times" were estimated for predicting the life of the polymer matrix composite components. However, the extensive testing was limited to tests on bulk HTPMC specimens. This methodology incorrectly presumes that there is no spatial variability in material response with aging and that the average response of the bulk material controls the life performance of the material.

The extraordinary cost of developing empirically-based design allowables and life prediction models for new material insertions is prohibitive when the cost must be amortized over only a few low-rate production aircrafts/spacecrafts. Currently, mechanism-based models and analyses used to predict the performance and life expectancy of HTPMCs are under development within the community of composite mechanics [**8**,**9**,**10**,**11**]. It is expected that these analyses and models will likely shed some light on the mechanisms controlling structural degradation and deformation

behavior due to thermal oxidation. The framework of these analyses can be summarized as a multi-scale program, as illustrated in Figure 1-1. It consists of experimental studies to characterize the surface degradation and mechanical behavior of constituent materials, analytical/numerical modelling to establish constitutive relation between microstructures (including fiber, matrix, and interphase), and finally the ply-level mechanical response as a function of thermal oxidation under aging conditions reflective of the in-service conditions. The success of the multi-scale modelling and analysis relies on the experimental capability of properly characterizing the evolution of mechanical behavior of each constituent under the aging conditions, in which the typical dimension of the constituents varies from submicron to millimeter and the HTPMCs display heterogeneous microstructures due to thermo-oxidative aging.

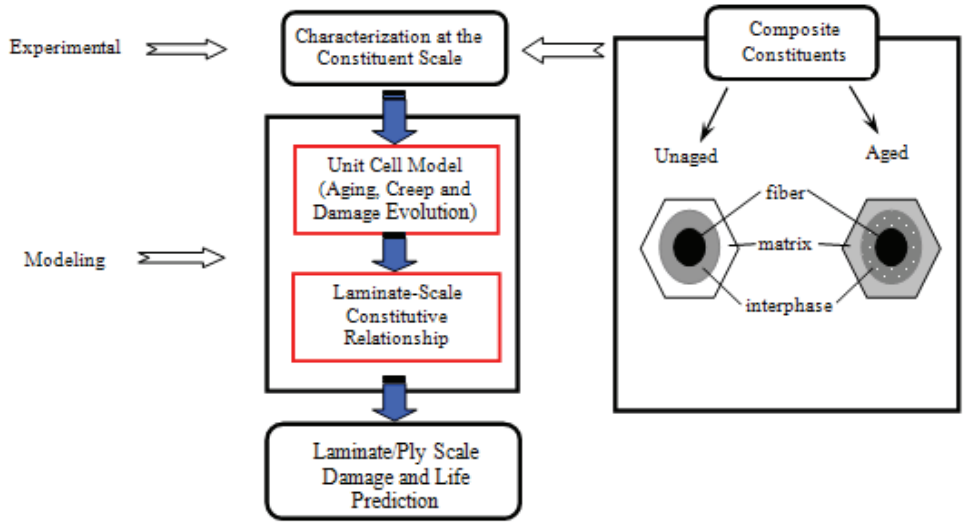

Figure 1-1 Schematic of the research for understanding the mechanical behavior of HTPMCs and predicting the life expectance of HTPMCs-based structures.

The nanoindentation technique has been very well recognized as a small scale test for characterizing the mechanical properties of materials in micron and submicron dimensions. It employs high-resolution actuators and sensors to continuously control and monitor the loads and displacements on an indenter as it is driven into and withdrawn from a material. From the load-displacement data, many useful engineering properties can be extracted. Although the nanoindentation technique has been used to measure the

local mechanical properties of materials/structures for over two decades, the work has been mostly limited to purely elastic materials. Fewer studies exist on the use of nanoindentation to examine the mechanical properties of time (rate) dependent materials such as polymers and polymer matrix composites.

1.2 OBJECTIVES OF THE THESIS

The key to predicting the lifetime and structural reliability of HTPMCs at elevated temperatures and improve the mechanical performance of HTPMC-based structures is to study and understand the physical and mechanical properties of HTPMCs at the constituent level upon thermal aging. A clear understanding of the complexity and nature of the thermal oxidation and its effects on local mechanical behavior will lead to the development of new and improved HTPMCs and better design methodologies for their applications. In this thesis, the mechanical properties of the HTPMC's matrix constituent, the polymer resin, were measured using a novel high-temperature nanoindenter. Specimens of PMR-15 polyimide, a legacy polyimide system used in aerospace and space applications, were processed and subsequently isothermally aged at various environmental conditions reflective of the in-service conditions. The objective of this project is to characterize the elastic moduli of the thermo-oxidatively aged samples using a newly developed high temperature nanoindenter. The data will be used to support the analytical/numerical models for predicting the life expectancy and damage of the polymer matrix composites for high-temperature applications.

1.3 ORGANIZATION OF THE THESIS

Chapter 2 (Review of Literatures) cites the publications that address the existing methods for characterizing the chemical/physical and mechanical properties of thermo-oxidatively aged HTPMCs. Chapter 3 gives a detailed description of the high temperature nanoindentation apparatus used in the project. Chapter 4 details the work on the nanoindentation testing and analysis of unaged PMR-15 resin, and a new method is proposed for analysing the nanoindentation data obtained from polymeric materials. Chapter 5 details the work on the nanoindentation testing and analysis of thermo-oxidatively aged PMR-15 resin. Chapter 6 summarizes the overall results and gives in brief the possible future work.

CHAPTER TWO REVIEW OF LITERATURES

2.1 INTRODUCTION TO PMR-15 POLYIMIDE RESIN

When designing an aircraft, a rocket, or an orbital vehicle, one of the primary design drivers is the total system weight. This parameter has a direct effect on a vehicle's range and payload capacity, performance and maneuverability, operational or launch costs, and in some cases mission feasibility. As a result, the aerospace industry is perpetually searching for lighter, stronger materials to incorporate into designs, most recently focusing on composite materials due to the ability to custom tailor their mechanical properties through constituent selection and geometric configuration within the material.

The most common family of composites used in aerospace are the polymer matrix composites (PMCs), which can vary greatly depending on the fiber reinforcement constituent, but have in common a polymeric resin matrix. While in lower performance applications it is possible to use the matrix as the load-bearing constituent material, in high-performance structural applications the fibers carry the load and are thus responsible for the composite's stiffness and strength whereas the matrix plays a secondary role as a load transfer mechanism while protecting and supporting the fibers.

In the 1960's and 1970's NASA and other aerospace research organizations began experimenting with new types of polymers that could withstand temperatures above 200°C, the service temperature limit of most epoxy resins used at that time [**12**]. Thermoset polymers are the most predominantly used matrix system in aerospace applications. Characterized as having a highly cross-linked structure that forms during the curing process, thermosets cannot be reshaped after their original formation and decompose thermally at high temperatures. The most commonly used types of thermosets include unsaturated polyesters, epoxies, vinyl esters, and polyimides. While the epoxy families frequently used in missile and aircraft structures typically display the most desirable mechanical properties of the thermoset polymers, polyimides are able to survive the higher service temperatures required by the new aerospace needs. Because of this, polyimides became the predominate resin system used in developing the high-

performance composites used in the industry today, and intensive research led to a new class of polyimides, polymerization of monomeric reactants (PMR).

In the mid-1970's, NASA Lewis Research Center developed PMR-15, a neat matrix resin which offers stable performance at high temperatures in addition to low cost and ease in processing (Figure 2-1, [**5**]). Since that time, PMR-15 has become the most widely used matrix in HTPMCs due to its thermo-oxidative stability and high glass transition temperature, T_g ~340°C, which permits composites having an extended service temperature of 288°C.

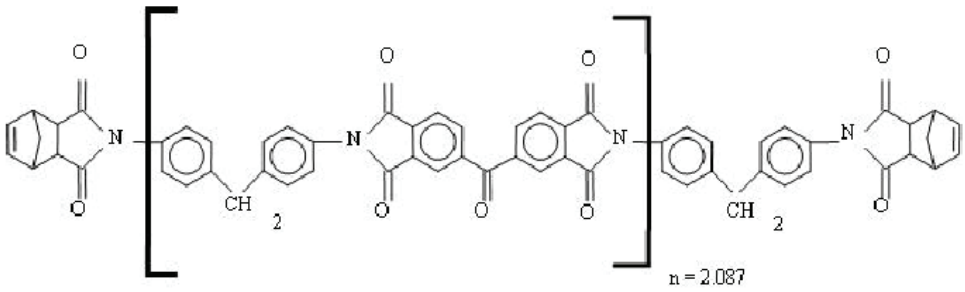

Figure 2-1 Stoichiometry of PMR-15 Resin ($MW_{theoretical}$ = 1500). Meador et al, [**5**].

In comparison to other resins of its type, "PMR-15 displays the best overall balance of processing, behavior, oxidative stability, and retention of mechanical properties" at high temperatures [**10**]. PMR-15 has been used to fabricate various engine components ranging from small compression-molded bearings to large structural autoclave-molded engine ducts used on the F404 engine for the U.S. Navy F-18A Hornet [**11**]. Today, PMR-15 has been recognized as the leading polymer matrix resin for carbon-fiber-reinforced composites used in aircraft engine components.

Because of its widespread use in the engineering community, PMR-15 has become perhaps the most extensively studied polyimide to date. Although current development efforts are focusing on replacing PMR-15 with another resin having higher service-temperatures and producing less carcinogenic by-products during initial manufacturing, it remains as the predominate resin system used in aerospace industry today. In response, current research in determining degradation mechanisms and in developing thermo-

mechanical property evaluation techniques, while extensible to other polymers, is still heavily focused on PMR-15 [**12**,**13**,**14**,**15**].

2.2 THERMO-OXIDATIVE DEGRADATION OF PMR-15 RESIN

One of the biggest problems in using HTPMCs today is the thermo-oxidative degradation of the polymer matrix as the materials are used at high temperature applications. Exposed to elevated temperature, the free surfaces of HTPMCs are susceptible to oxidation. And when exposed to thermo-mechanical loading, the result is accelerated degradation and ply cracking which in turn introduces new free surfaces, exacerbating the problem. Ultimately, this leads to degradation of the fiber-matrix interfaces, reducing the life and durability of the composite system. Thus the ability to fully understand and characterize the physical and chemical responses resulting from thermo-oxidative processes is paramount to the continued development and increased use of HTPMCs in the aerospace industry.

The thermo-oxidative degradation of PMR-15 has been studied recently. Putthanarat, et al. [**16**], defined oxidative aging of PMR-15 as "a nonreversible, surface diffusion response in which chemical changes occur during the oxidation of a polymer, [where] oxidation leads to a reduction in molecular weight as a result of chemical bond breakage and weight loss due to out-gassing of low-molecular weight gaseous species." Meador et al [**5**] have studied the chemical structures of oxidized PMR-15 using nuclear magnetic resonance (NMR) spectroscopy. It was found that the end-caps of the molecular chain in PMR-15 have changed after thermo-oxidative aging (Figure 2-2). These chemical structural changes are believed to accounted for much of the weight loss of the resin aged in air at elevated temperatures. Xie et al [**17**] and Patekar [**18**] have used the Fourier-Transform Infrared (FTIR) spectrometer to study the aged PMR-15 and found that many by-products are released from PMR-15 as a results of thermo-oxidation, including H_2O, CO, CO_2, CH_4, and NH_4 .

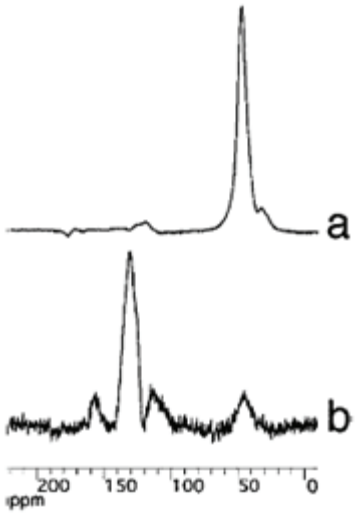

Figure 2-2 NMR difference spectra of PMR 15 labelled on the nadic end cap, (a) as cured and (b) after aging as a powder for 64 h at 315 °C in air, Meador et al, [**5**].

Due to the changes in chemical structure, the surface layer near the specimen edges exhibits different optical characteristics than the interior of the specimen. Using bright-field light microscopy, Schoeppner et al [**3**] have observed that the oxidized material has a different appearance than the unoxidized interior (Figure 2-3). The figure clearly shows the oxidized region (much like a picture frame) on the two adjacent exposed free surfaces of the specimen. Between the outer oxidized layer and the interior unoxidized region is a transition region. Tandon et al [**1**] have thus proposed a three-region model for the thermal oxidation of PMR-15. According to this three-region model, the oxygen (O_2) diffuses through the polymer, and is consumed by the oxidation reaction. Once a region is fully oxidized (the Oxidized Layer), the oxidation reaction is terminated and oxygen can diffuse through it. Then, oxidation begins to react in the adjoining region (the Transition Region). The region far from the exposed surface where no oxidation has occurred is called the Unoxidized Interior.

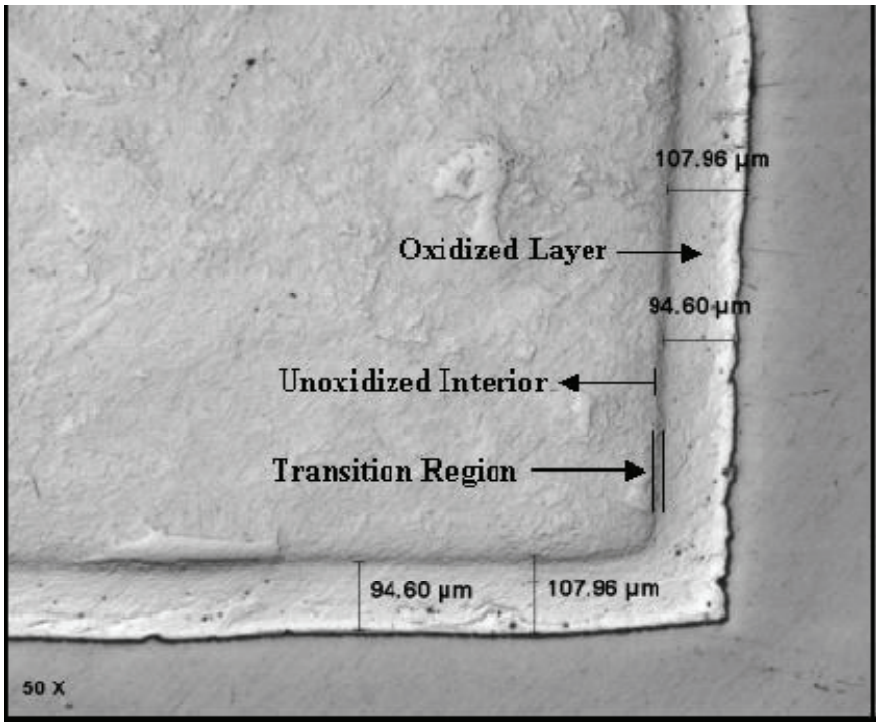

Figure 2-3 Photomicrograph of PMR-15 resin after 196 hours of aging at 343°C showing oxide layer formation, transition region, and unoxidized interior – Schoeppner et al, [**3**].

The thickness of the oxidized surface layer grows with oxidation. The magnitude depends upon the environmental conditions (time, temperature and pressure). Initially, the thickness of the oxidized layer increases rapidly with aging time and then the rate of change starts to decrease (Figure 2-4). This is because the oxidation growth rate decreases with time over longer aging time periods (Tandon et al. [**1**]).

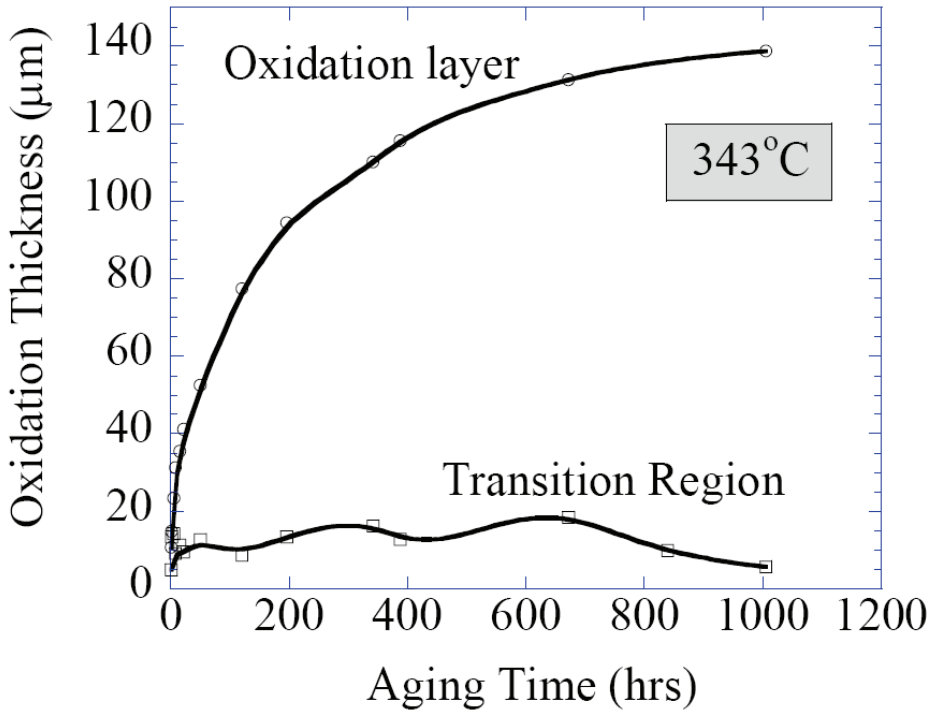

Figure 2-4 Evolution of oxidation layer and transition region thickness with aging time– Tandon, et al. [**1**].

Bowles et al [**19**], using metallography directly observed the surface of the thermo-oxidized PMR-15 resin. It is found that, at very high temperatures (>340°C), voids have formed in the surface layer and these voids can develop into microcracks over time. Meador et al [**5**] have examined oxidized PMR-15 using scanning electron microscopy and determined that the surface layer has much higher oxygen concentration than the unaged interior. The formation of the voids found in the surface layer is considered as a result of the Kirkendall effect. That is, the inward diffusion of oxygen is slower than outward diffusion of degradation products [**5**].

2.3 MECHANICAL CHARACTERIZATION OF THERMALLY OXIDIZED PMR-15 RESIN

The focus of the present work is the direct mechanical characterization of thermally oxidized PMR-15 polyimide. As such, a brief review of other mechanical characterization techniques is presented here. Early studies were mostly conducted through conventional mechanical testing methods by testing bulk specimens that consisted of both oxidized surface layer and unoxidized interior.

Tsuji et al. [**20**] have measured the elastic modulus of PMR-15 aged at 316°C in air and nitrogen for durations of up to 800 hr. Four-point bend tests were performed on specimens aged in nitrogen as well as air to determine the modulus of both the oxidized surface layer and the inner core material (Figure 2-5). The modulus of the "composite" specimens, E_c, is calculated according to ASTM D 790M:

$$E_c = \frac{0.17L^3m}{wt^3} \tag{2.1}$$

where L is the support span, w is the specimen width, t is the specimen thickness, and m is the slope of the tangent to the initial straight-line portion of the load-deflection curve.

The modulus of the oxidized surface layer, E_s, is extracted from E_c by using the basic beam theory:

$$E_s = \frac{1}{I_s}\left(\frac{L^3m}{96} - E_cI_c\right) \tag{2.2}$$

where L is the support span, m is the slope of the tangent to the initial straight line portion of the load deflection curve, and I_c, I_s, are the inertias of the whole specimen and the surface section, respectively.

By making the assumption that an oxidized specimen is effectively a bimaterial strip, behaving as a composite sandwich, classical beam theory was used to determine the elastic modulus and coefficient of thermal expansion of the unoxidized layer. In doing so, two important assumptions were made as to the nature of the oxidation layer and transition zone. The first is that the oxidized layer has uniform properties, and the second is that the oxidation front ends abruptly with no transition into the apparently unoxidized interior. A difficulty with this method is that while the experiment itself is mechanical in nature, an indirect calculation must be performed making potentially erroneous assumptions as to the nature of the measured specimen.

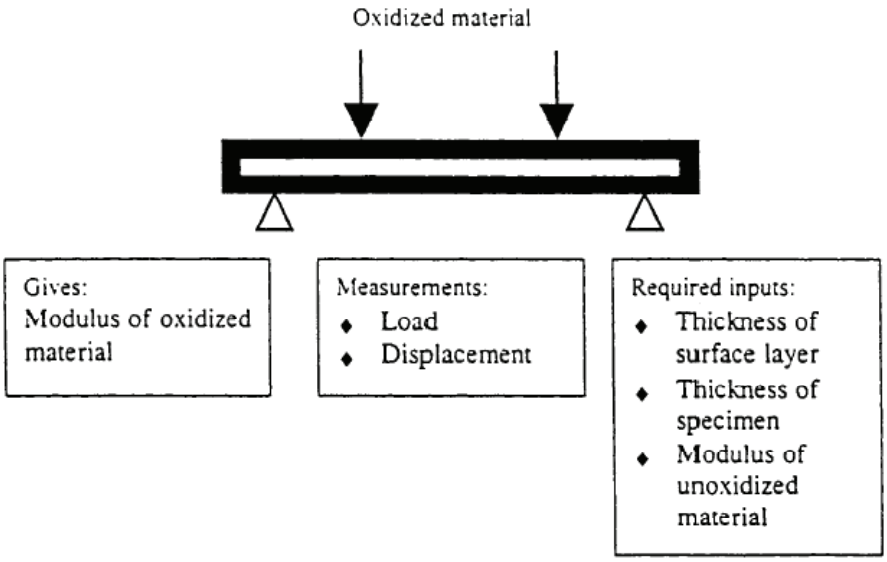

Figure 2-5 Four-point bend test schematics – Tsuji et al [**20**].

Recently, small-scale testing methods such as atomic force microscope and nanoindentation have been used to examine the properties of the oxidized materials. Johnson et al [**9**] have used an atomic force microscope equipped with a nanoindenter tip to study the effects of aging time and temperature on oxidation profiles in PMR-15 resin. Results confirmed that oxidized surface and unoxidized core had significantly different properties and also that the visible reaction zone is the diffusion-controlled oxidation zone, which is a result of a first-order reaction. Ripberger et al [**21**] and Putthanarat et al [**16**] have performed nanoindentation tests on thermo-oxidized PMR-15 specimens. The modulus of the material in the oxidized region is found to be higher toward its outer edge and decreases to the unoxidized modulus in the interior. The measured increase in stiffness near the specimen edge is consistent with embrittlement associated with aging the neat resin specimen in air.

The nanoindentation experiments mentioned above have been conducted and analyzed using the methodology that are mostly applicable to purely elastic materials. The time/rate effect in nanoindentation testing or analysis has not been considered, thus the modulus reported may not represent the true properties of the materials. In addition, the existing nanoindentation tests have been limited to ambient temperature conditions.

CHAPTER THREE OVERVIEW OF NANOINDENTATION APPARATUS

3.1 INTRODUCTION

This chapter begins with an overview of the nanoindentation testing theory, followed by a detailed description of the nanoindentation equipment used in the present project, along with the necessary hardware modifications needed to perform high temperature nanomechanical characterization experiments. Discussion of preliminary calibration techniques follows, noting in particular those areas where high-temperature measurement differs from traditional indentation techniques.

3.2 NANOINDENTATION TEST

The nanoindentation testing technique has been developed over the last two decades as a small scale test for characterizing the mechanical properties of materials in small dimensions or in localized regions [**22**,**23**,**24**,**25**,**26**,**27**,**28**]. Because indents can be positioned to within a few microns or less, this technique provides the ability to map the spatial distribution of surface mechanical properties with good resolution.

The principle of nanoindentation can be explained as follows: As an indenter is driven into and withdrawn from the testing material, the resultant load-displacement curve can be recorded continuously, as shown in Figure 3-1. It is assumed that during the initial unloading the deformation is purely elastic [**22**], thus, the slope of the initial portion of the unloading curve yields the elastic contact stiffness, *S*:

$$S = dP/dh \tag{3.1}$$

where *P* is the load and *h* is the displacement at the indenter tip.

Following Oliver and Pharr [**23**,**24**], the contact depth, h_c, can be further determined from the loading-unloading curve:

$$h_c = h\text{-}0.75P/S, \tag{3.2}$$

where *h* is the total indentation depth and *P* the maximum load.

Using the contact depth, the projected contact area, A, can be estimated through an empirically determined area function:

$$A = f(h_c) \tag{3.3}$$

Once the contact area is determined, the reduced modulus and hardness can be calculated as:

$$E_r = \frac{1}{\beta}\frac{\sqrt{\pi}}{2}\frac{S}{\sqrt{A}} \tag{3.4}$$

$$H = P/A \tag{3.5}$$

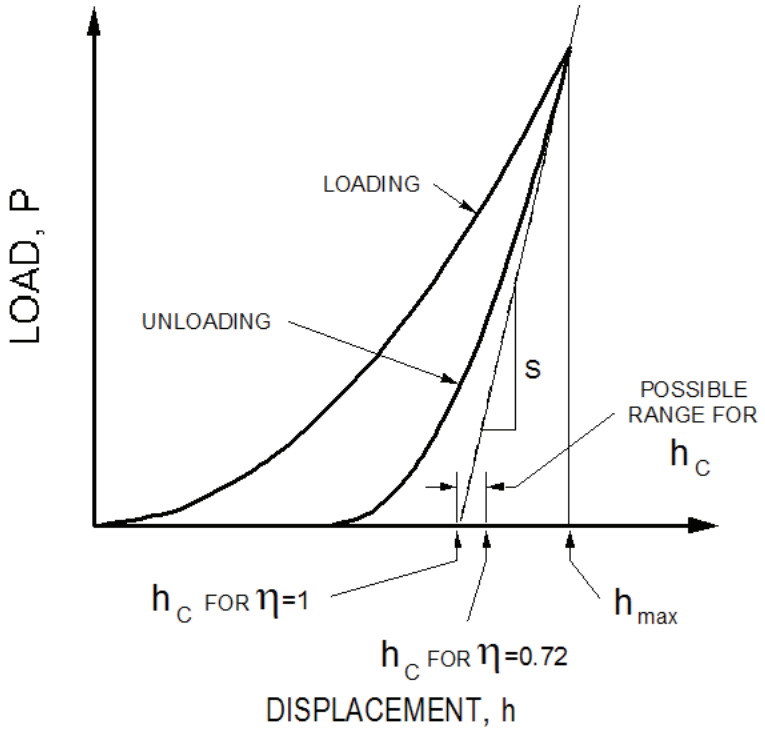

Figure 3-1 Schematic of typical load-displacement data defining key experimental quantities [**22**].

3.3 NANOINDENTATION APPARATUS

The nanoindentation apparatus used in the present work is centered around the MTS (Materials Testing System) Nano Indenter® XP, located at the Air Force Research Laboratory's Materials and Manufacturing Directorate, Wright-Patterson Air Force Base, Ohio. The MTS Nano Indenter is a microprobe used primarily to determine the local properties of Young's modulus and hardness, allowing for pinpoint measurements in

material samples having spatial property variations that cannot be quantified using more conventional bulk property determination methods.

The workhorse of the indentation apparatus is the indenter head assembly as shown in Figure 3-2, supported by two leaf springs, thus having very low vertical stiffness while maintaining very high horizontal stiffness. The indenter shaft is essentially a load-controlled solenoid armature, passing through an electromagnetic coil. The load force is then directly proportional to the current passed through the coil, resulting in known loads with a theoretical resolution of 50 nN. Displacement measurement is determined by a capacitive displacement sensor consisting of three vertically-concentric circular disks. By observing the electric potential across the center and either of the outer plates, the vertical displacement can be determined to a theoretical resolution of less than 0.01 nm [**22**].

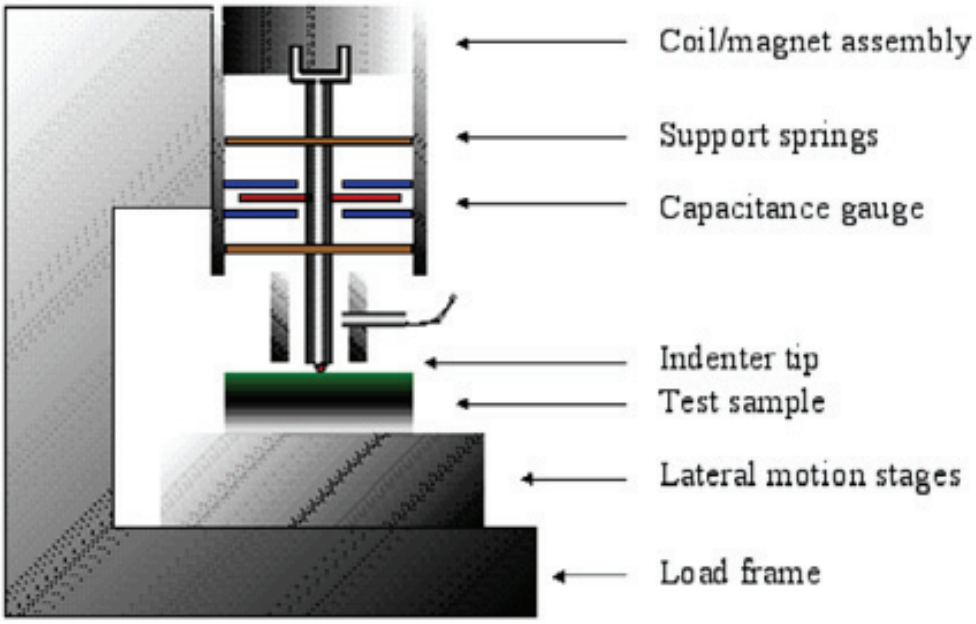

Figure 3-2 Schematic detailing indenter head assembly, MTS [**22**].

The heart of the MTS Nano Indenter® XP is the gantry used to support the indentation, optics, and motion systems (Figure 3-3); the gantry is manufactured to be extremely rigid, providing the system with a very high load frame stiffness, crucial to the nanoindentation method [**22**].

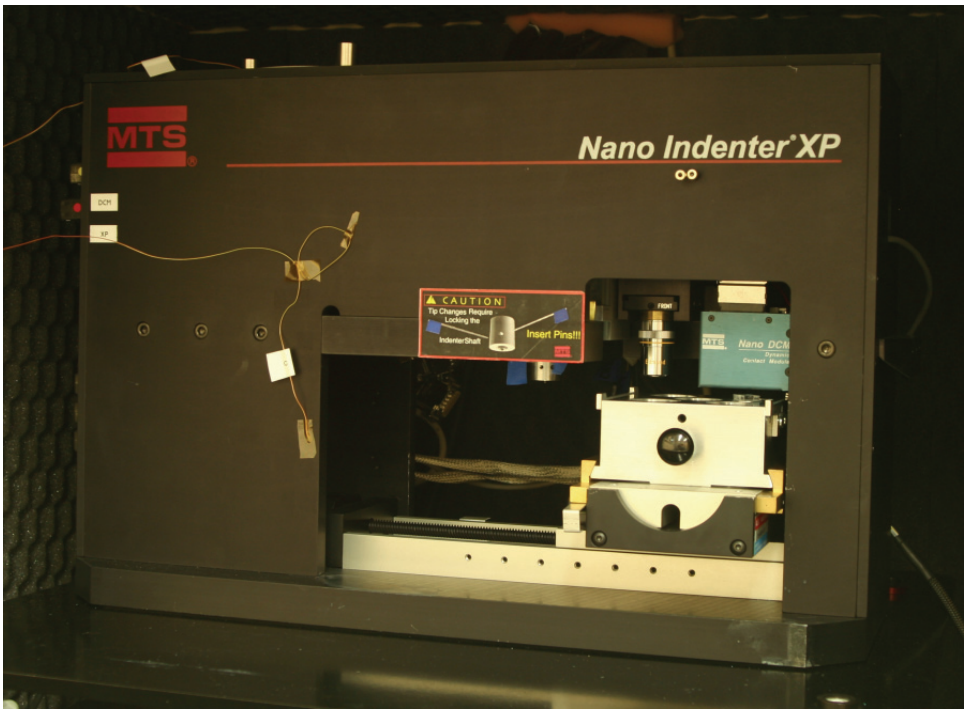

Figure 3-3 MTS Nano Indenter® XP Gantry shown here in its base configuration, along with DCM module, which must be removed in high-temperature configuration.

The gantry shown above is mounted on an MTS Minus K Table in an isolation cabinet, used to retard environmental temperature changes and acoustic disturbances. The isolation cabinet provides a stable air mass to minimize sudden temperature changes within the enclosure while its interior foam lining serves to absorb acoustic energy and decreases the acoustic transmission to the instrumentation [**22**]. The Minus K Table, mounted inside the vibration isolation cabinet (Figure 3-4), provides a level surface on which to mount the gantry, providing a highly decoupled system having a natural frequency at or below 0.6 Hz [**25**]. In addition, the table's Nano-K auto-adjust system provides a means for an initial active damping and monitoring of the gantry's harmonic oscillations.

Figure 3-4 The Minus K Table (Left) minimizes external vibration excitations. The Nano-K auto-adjust system (Right) provides initial active damping and monitoring of harmonic oscillations, MTS [**22**].

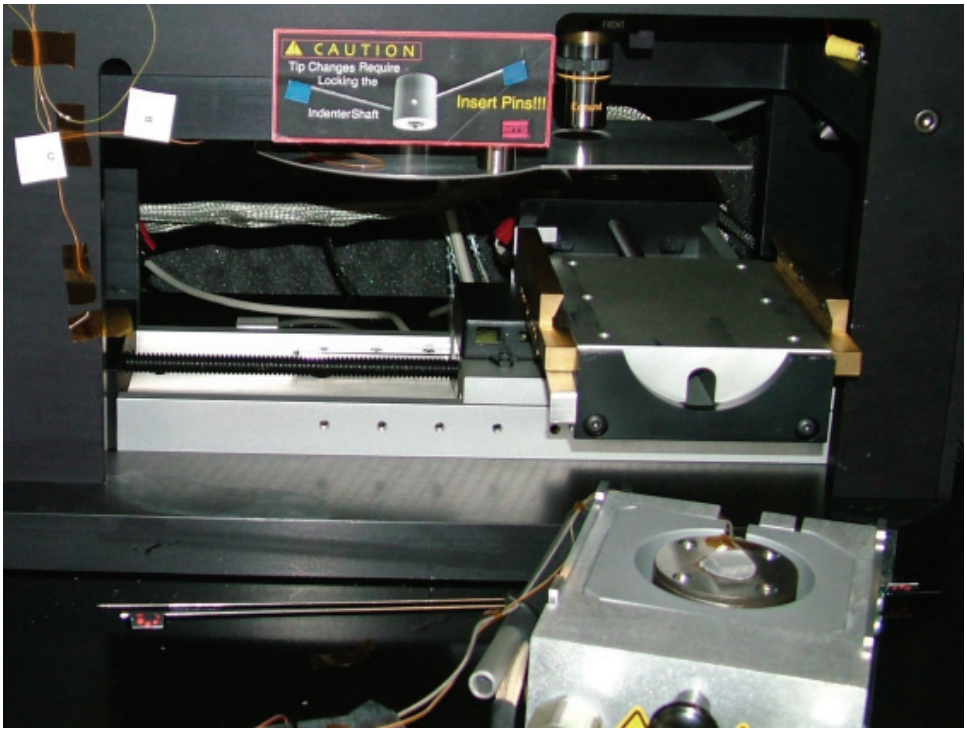

Figure 3-5 The essential components of the nanoindentation system.

Located inside the gantry are all of the primary indentation mechanisms, comprising of the horizontal motion system, optics system, indenter head assembly, and sample mount system (Figure 3-5). The software-controlled motion system consists of X-Y directional positioning stages, their respective motors, and gearboxes that interface via an encoder

that transfers data to and from the externally located expansion chassis, which houses and powers the data acquisition and control electronics (Figure 3-6). “The translation stages are screw-driven and the theoretical resolution for site selection is 45 nm with a real accuracy of ≈ 1.5 μm….The motion of this stage is guided by highly pre-loaded, crossroller bearing slides that provide excellent linearity and stiffness” [**22**].

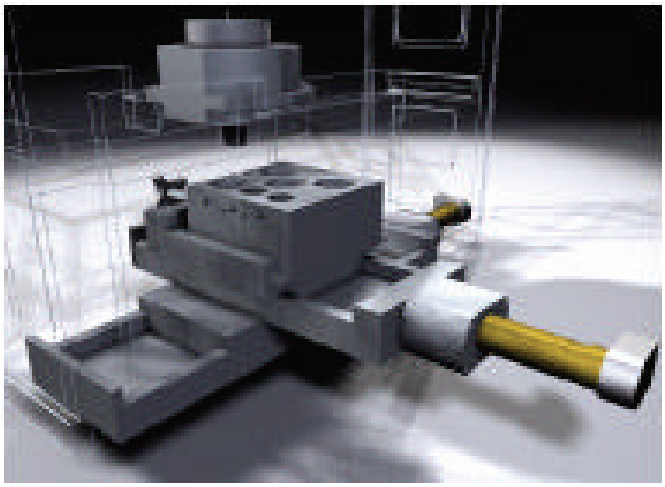

Figure 3-6. Screw-driven X-Y directional stages are mounted to the gantry base, MTS [**22**].

The optics system is comprised of a microscope body, interchangeable 10X and 40X magnification objective lenses, a video camera, a computer driven optics focus motor, and an adjustable iris diaphragm. A remotely located halogen light source with adjustable intensity transmits light to the microscope body via fibre optic cable, to provide localized illumination to the specimen surface (Figure 3-7).

Figure 3-7 The microscope body and components (Left) are mounted inside the gantry, while the illuminator (Right) transmits light via fibre optic cable, MTS [**22**].

The nanoindentation tests have been mostly performed at ambient temperature. In order to perform high-temperature testing, the nanoindenter configuration must be outfitted with additional components. A stainless steel heat shield (Figure 3-8) must be installed to protect the sensitive optics and indentation systems from thermal damage (if the DCM (dynamic contact module) module is installed, it must be removed as well).

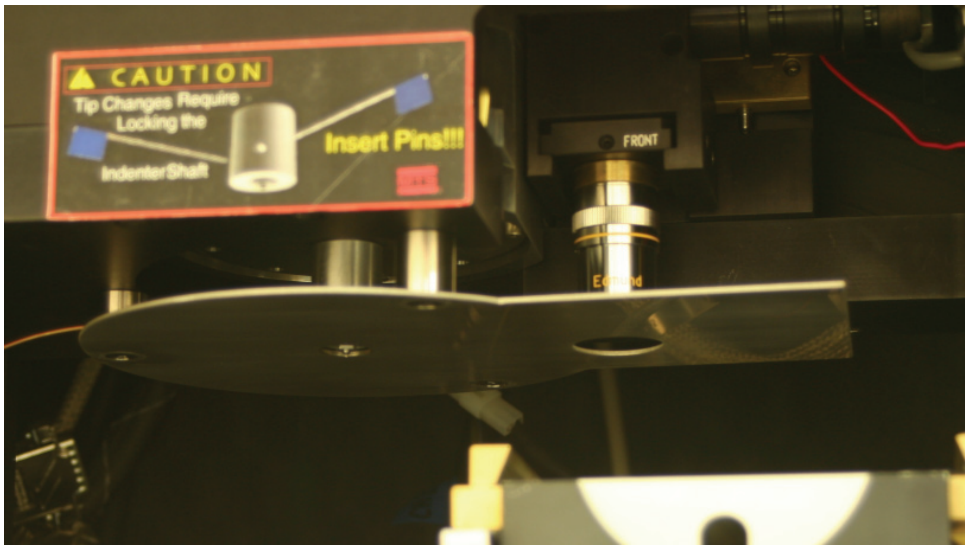

Figure 3-8 Heat shield as installed.

In addition, a heating source is needed to conduct high temperature experiment. The sample stage used throughout this experimentation is the MTS Localized High Temperature Stage [**26**]. The stage consists of a plated copper sample puck which is attached to a stack of two heater plates by four screws as seen in Figure 3-9 . This heater core stack is permanently mounted in a ceramic isolator, which attaches to an aluminium stage by means of a compression fit achieved by tightening a bolt through the aluminium block. The aluminium block is fitted with two coolant ports which allow a thermal coolant to be pumped through the block by an external coolant pump (Figure 3-10), thereby minimizing the thermal effects on the surrounding system. The heater core stack is powered and monitored by a variable DC output proportional controller (J-KEM Scientific, Inc.) (Figure 3-10).

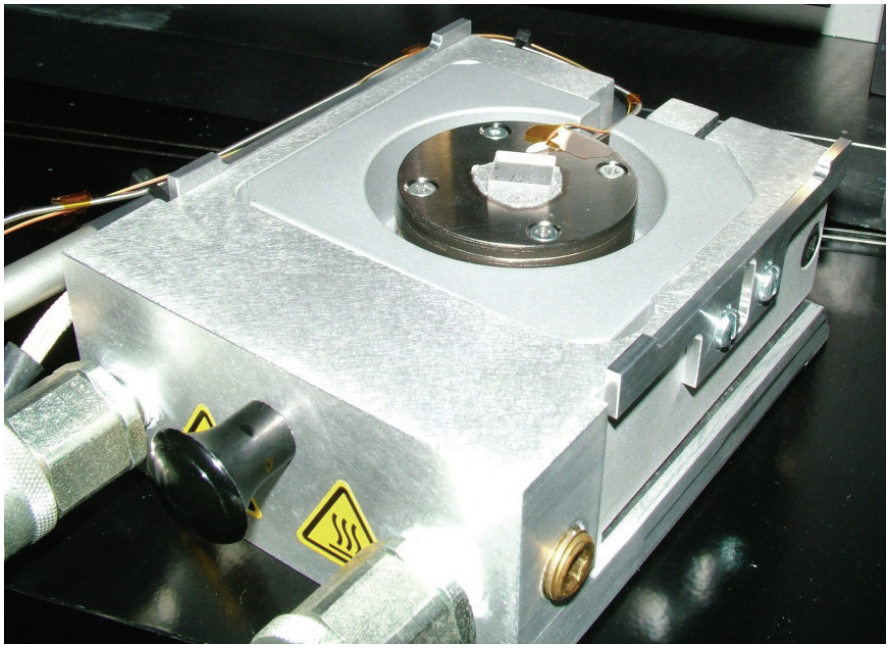

Figure 3-9 MTS Localized High Temperature Stage.

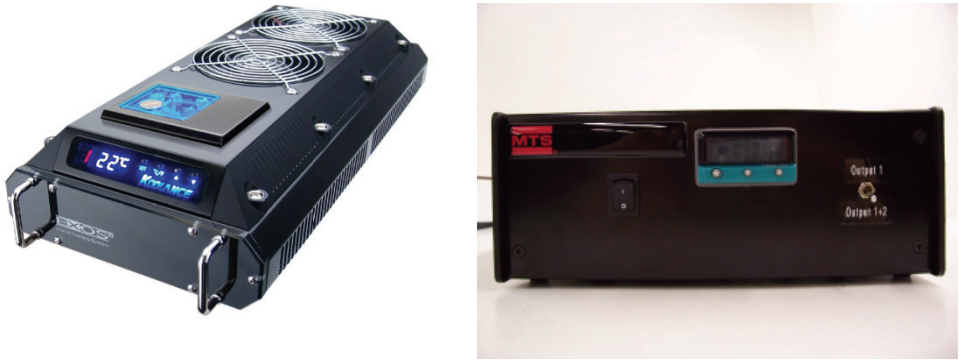

Figure 3-10 The Koolance Exos-2 pump (Left) cools the aluminium block. The J-KEM temperature controller (Right) powers the two heater cores.

Additional temperature monitoring was logged using thermocouples connected to a National Instruments CompactDAQ data acquisition system (Figure 3-11). These additional thermocouple readings allowed for temperatures to be monitored in various locations throughout the system in real-time using LabVIEW, quantifying the thermal characteristics of the system as a whole throughout the testing procedure.

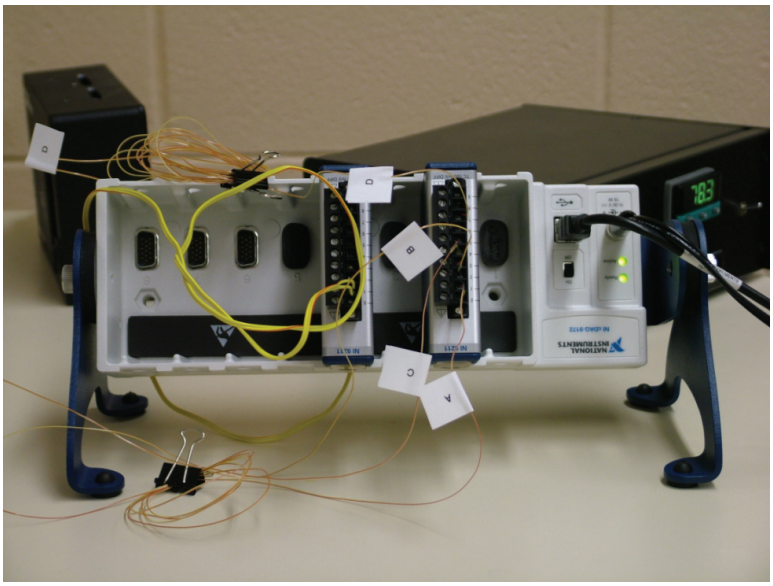

Figure 3-11. National Instruments CompactDAQ was used with Labview software to quantify thermal characteristics of the system during testing.

3.4 EQUIPMENT CALIBRATIONS

To conduct nanoindentation tests at elevated temperatures, the apparatus needs to be calibrated to ensure that the stiffness of the machine is not significantly affected by the change of temperature. Fused silica (amorphous SiO_2) was used as a reference calibration standard for nanoindentation, as it is relatively inexpensive, has a smooth surface free from oxidation, and has mid-range isotropic mechanical properties. The fused silica samples obtained from MTS measure approximately 12 mm x 12 mm x 2.5 mm in thickness and have a nominal elastic modulus of 72 GPa. These pre-prepared samples are then mounted to the copper "puck" with a high temperature adhesive that has similar thermal expansion properties of the sample tested (Figure 3-12).

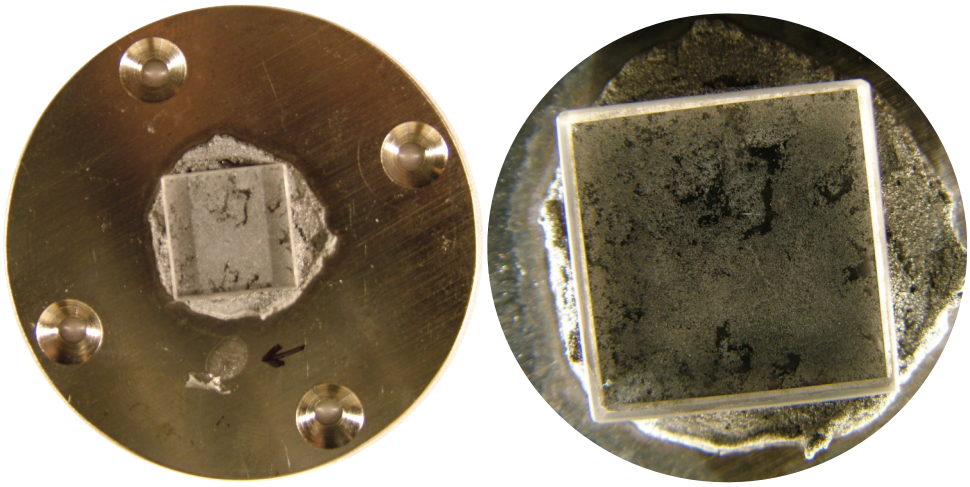

Figure 3-12 Fused silica calibration standard shown mounted on the copper puck, (Left), and close-up of same sample (Right).

The fused silica samples were tested on the present MTS nanoindenter from room temperature up to a temperature of 250°C. The modulus of the material was calculated using standard Oliver-Pharr equation and the results are seen in Figure 3-13. It is seen that the modulus of the fused silica remains relatively unchanged over the temperature range of interest. The trend is consistent with the data from the literature [**27**,**28**]. The results indicate that the present MTS nanoindenter is relatively stable and no correction in machine frame stiffness is needed in the modulus calculation.

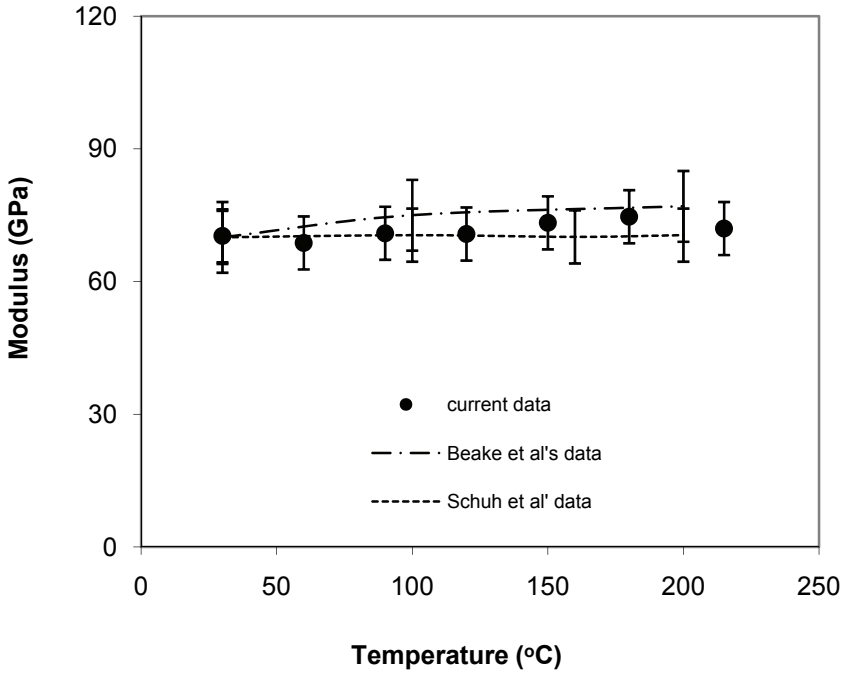

Figure 3-13 Variations of elastic modulus of fused silica as a function of temperature.

CHAPTER FOUR NANOINDENTATION TESTING OF UNAGED PMR-15 POLYIMIDE

4.1 INTRODUCTION

This chapter presents the high temperature nanoindentation experiments performed on unaged PMR-15 polyimides. The sharp-tipped Berkovich nanoindenter equipped with a hot-stage heating system was used. The indentation experiments were performed using the "hold-at-the-peak" method at various indenter holding times and unloading rates. The creep effect was seen to decrease with increasing holding time and/or unloading rate. Procedures used to minimize the creep effect are investigated at both ambient and elevated temperatures so that the correct contact depth (together with modulus and hardness) can be determined from nanoindentation load-depth curve. The temperature dependent mechanical properties of PMR-15 are measured through the current nanoindenter and results are consistent with those obtained from macroscopic tests.

4.2 EXPERIMENTAL TECHNIQUE

4.2.1 MATERIALS

Rectangular unaged PMR-15 neat resin plaques were compression molded using a steel die based on the processing parameters provided by manufacturer. The plaques were then post-cured in air for 16 hr at 316°C. Smaller specimen (100 mm x 100 mm x 2 mm) was subsequently cut from the plaque using a diamond saw with distilled water as a cooling media. The specimen was washed using a common household soap and then rinsed with distilled water for a minimum of 5 min. Rubber gloves were worn throughout while handling the sample in order to prevent contamination of specimens from oils, etc. The specimen was then dried with standard paper towels and placed in a vacuum oven at 105°C for a minimum of 48 h to remove any moisture within the samples, and stored in a nitrogen purged desiccator until testing. The specimen was then potted in Jeffamine 828-D230 epoxy resin that was cured at room temperature for three days. The surface of the specimen was prepared by grinding papers and polishing compounds, the final polishing compound being alumina with an average particle size of 0.3 μm. The potted specimen

was used for surface profiling, optical microscopy measurements and nanoindentation testing.

4.2.2 EQUIPMENT

The high-temperature nanoindentation tests were performed on a Nano Indenter XP equipped with thermal control system (MTS NanoInstruments, Oak Ridge, TN). The thermal control system consists primarily of (a) a hot-stage assembly positioned below the test specimen, (b) a stainless steel heat shield that is used to isolate the indenter transducer assembly from the heat source, (c) a coolant system that is used to remove heat from the surrounding stage, and (d) a temperature controller. The hot-stage assembly is an aluminum stage holder containing a resistance-type microheater, a coolant port and a ceramic isolator. The temperature of the hot-stage can be set up to 400°C by using an electronic controller and monitored by a LabView data acquisition system through a J-type thermocouple embedded inside the hot-stage. The PMR-15 specimen was mounted to a special sample disk using a high-temperature adhesive (Poly-2000). This adhesive is designated for extreme temperature applications, up to 1090°C, and possesses a minimum amount of thermal expansion.

The Berkovich diamond indenter was used in the present experiments. The indenter has a nominal tip radius of $r < 20$ nm and an inclined angle of $\theta = 65.3°$. The latest tips provided by the manufacturer had all been brazed onto the tip holder, a process allowing tips to be used at elevated temperatures. The entire tip assembly was attached directly to the force transducer which is behind the installed heat shield. To minimize the distribution of heat into the entire testing system, the specimen (mounted on the hot-stage) was heated outside the machine and then brought in contact with the indenter tip. As the hot specimen was in contact with a cold tip, rapid heat transfer occurred. Additional time (~60 min.) was given for redistribution of heat to ensure the indenter-specimen system equilibrated at the given test temperature. The thermal drift rate used was 0.1 nm/s. After each temperature experiment, the tip was cleaned to ensure that it was not contaminated by heated polymer samples. The applied load and penetration depth were recorded during each test and used to compute the modulus and hardness of the materials.

4.3 DATA ANALYSIS

Polymers exhibit time-dependent viscoelastic deformation, i.e., creep, particularly at elevated temperatures. It is known that during the nanoindentation of a viscoelastic material, the resultant load–displacement plot may exhibit a "nose" (or a "bulge") in the initial unloading segment due to excessive creep. When a "nose" occurs, the resultant contact stiffness will be negative [**29**,**30**,**31**,**32**]. To reduce the creeping effect (as well as other effects such as instrument drift) on the unloading set of data, a technique called "hold-at-the-peak" has been recently adopted for nanoindentation testing of polymers [**29**,**30**,**31**,**32**]. That is, the indenter is held at the maximum load for a length of time prior to unloading, a procedure allowing the material to relax and provoking the disappearance of the "nose". Once the apparent "nose" is eliminated from the initial unloading curve, the elastic contact depth can be estimated from the indentation load-depth curve through a modified Oliver-Pharr equation [**32**].

$$h_c = (h_{\max} - h_{creep}) - 0.75\frac{P_{\max}}{S_e} \tag{4.1}$$

where $h_{\max}$ is the maximum indentation depth and h_{creep} the change in the indentation depth during the holding time. $P_{\max}$ is the peak load and S_e the elastic contact stiffness. According to Ngan and Tang [**29**], the total displacement under the indenter at the moment of unloading can be decomposed into elastic component, h_e, and creep component, h_v, based on a simple spring-dashpot model. Thus, the elastic contact stiffness, S_e, can be determined from the apparent stiffness, S, as follows

$$\frac{1}{\mathrm{S}} = \frac{\partial \mathrm{h}}{\partial \mathrm{P}} = \frac{\partial(\mathrm{h_e} + \mathrm{h_v})}{\partial \mathrm{P}} = \frac{\partial \mathrm{h_e}}{\partial \mathrm{P}} + \frac{\dot{\mathrm{h}}_{\mathrm{v}}}{\dot{\mathrm{P}}} = \frac{1}{\mathrm{S_e}} + \frac{\dot{\mathrm{h}}_{\mathrm{v}}}{\dot{\mathrm{P}}} \tag{4.2}$$

or

$$\frac{1}{\mathrm{S_e}} = \frac{1}{\mathrm{S}} - \frac{\dot{\mathrm{h}}_{\mathrm{v}}}{\dot{\mathrm{P}}} \tag{4.3}$$

where S is the apparent stiffness that is determined from the slope of the unload curve evaluated at the maximum depth ($S = (dP/dh)_{h=h_{\max}}$), $\dot{h}_v$ is the creep rate at the end of the

load hold and $\dot{P}$ the unloading rate. Substituting Equation (4.3) into Equation (4.1), the correct contact depth is determined by [**41**]

$$h_c = (h_{max} - h_{creep}) - 0.75 P_{max} \left(\frac{1}{S} - \frac{\dot{h}_v}{\dot{P}}\right) \tag{4.4}$$

Once the correct contact depth is known, the indenter-sample contact area, A, can be estimated through a tip-area function. The tip-area function is an experimentally determined function of the contact depth, h_c, expressed as follows

$$A = C_0 \cdot h_c^2 + \sum_{i=1}^{n} C_i \cdot h_c^{1/2^{(i-1)}} \text{ , n=8 or less} \tag{4.5}$$

where C_0 and C_i are coefficients determined through a calibration process on reference materials (high-purity fused silica) provided by the MTS. The first term, C_0, would be the area versus contact depth for a perfectly sharp Berkovich indenter while the following terms, C_i, account for tip bluntness.

After estimating the indenter-sample contact area, A, the elastic modulus, E, and hardness, H, can be calculated following the standard procedures (4.6)(4.7)

$$E = \frac{1-\nu^2}{\frac{1}{E_r} - \frac{1-\nu_i^2}{E_i}} \tag{4.6}$$

$$H = P_{max}/A \tag{4.7}$$

where $E_r = \frac{\sqrt{\pi}}{2 \cdot (1.034)} \frac{S_e}{\sqrt{A}}$, and E_i and ν_i are the elastic modulus and Poisson's ratio of the indenter (for diamond indenter: $E_i = 1140$ GPa and $v = 0.07$).

4.4 RESULTS AND DISCUSSION

4.4.1 CREEP EFFECT IN NANOINDENTATION OF POLYMERS

PMR-15 is a thermoset polymer and known to exhibit viscoelastic creep, particularly at elevated temperatures. The standard nanoindentation test is based on the assumption that the deformation during initial unloading is purely elastic. Thus, by curve-fitting the slope of the initial unloading curve, the elastic contact stiffness, S_e, can be computed, from which the contact depth, h_c, and elastic modulus, E, are calculated. When indenting a material exhibiting time-dependent deformation, errors may occur in determining the contact stiffness and contact depth using the same method (due to the presence of viscoelastic creep at the initial unloading). To minimize the creep effect, the present experiments were performed using the "hold-at-the-peak" method, a procedure proposed by some researchers for indenting viscoelastic materials [**29**,**30**,**31**,**32**]. In the tests, the indenter was loaded at a maximum load, held at the peak for a length of time and then unloaded. Various indenter holding times and unloading rates were used to investigate the creep effect.

Figure 4-1, Figure 4-2 and Figure 4-3 show the indentation load-depth responses of PMR-15 at ambient temperature (T= 23 ± 0.5°C). In each test, the PMR-15 specimen was indented using the "hold-at-the-peak" method under increased load up to a maximum of 500 mN. The holding times in Figure 4-1, Figure 4-2 and Figure 4-3 are 2 s, 20 s, and 120 s, respectively. It is observed that while held at constant load, the indenter continues to penetrate into the specimen, an indication that the present PMR-15 material undergoes creep deformation even at ambient condition. For comparison, the high purity fused silica, a linear elastic material, was tested under the same conditions (with holding times of 2 s, 20 s and 120 s). As an example, the load-depth curves under a 20 s holding time are shown in Figure 4-4. It is seen that no visible creep has occurred on fused silica, which is consistent with the results reported by Beake and Smith [**27**].

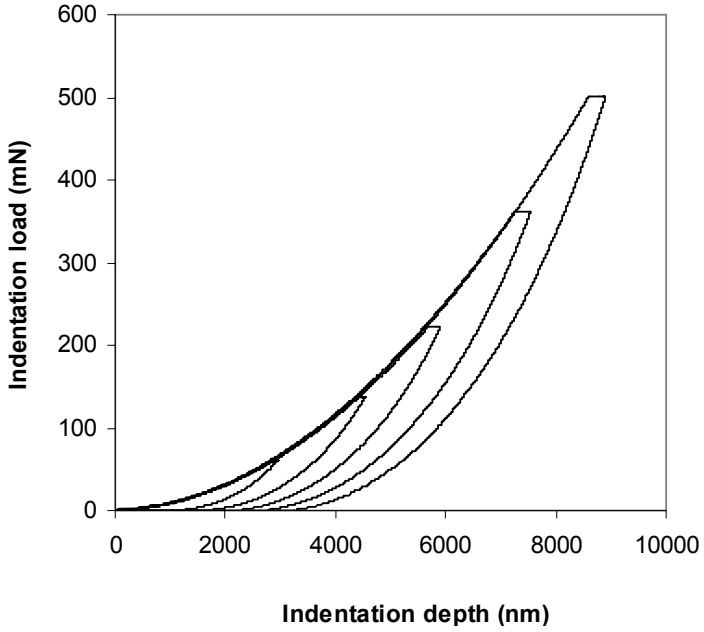

Figure 4-1 Indentation load-depth curves of PMR-15 polyimide with a holding time of 2 s.

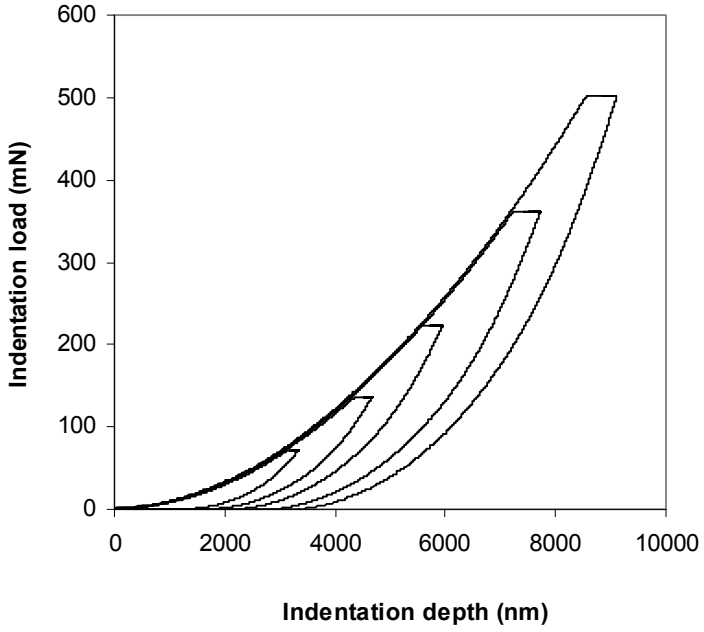

Figure 4-2 Indentation load-depth curves of PMR-15 polyimide with a holding time of 20 s.

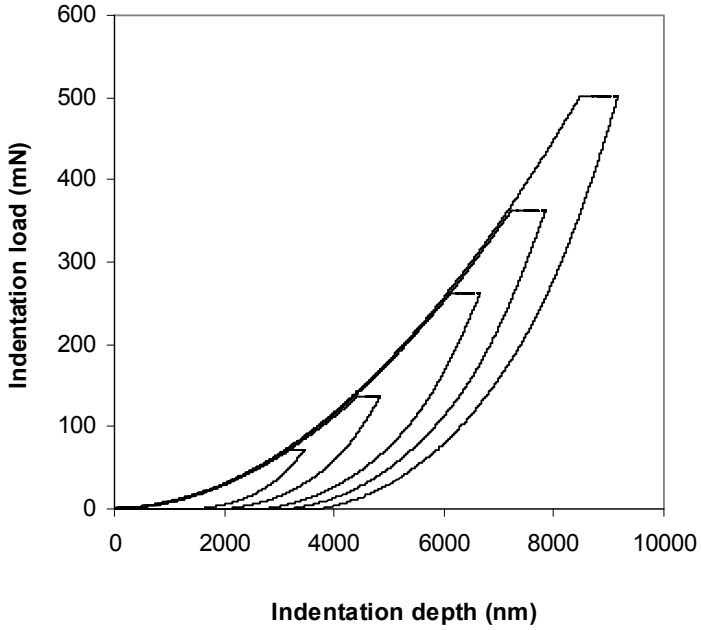

Figure 4-3 Indentation load-depth curves of PMR-15 polyimide with a holding time of 120 s

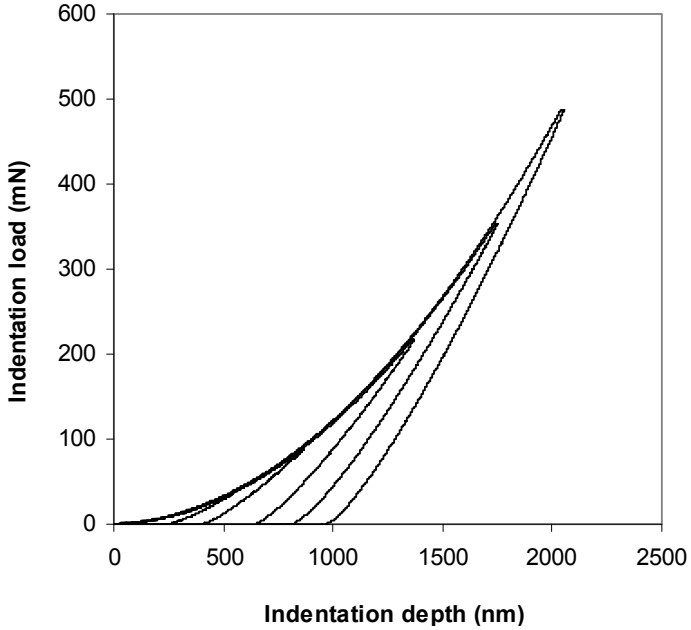

Figure 4-4 Indentation load-depth curves of fused silica with a holding time of 20 s

As the holding time increases from 2 s to 120 s, the creep distances increase as expected (Figure 4-1, Figure 4-2 and Figure 4-3). The amount of creep also increases with the increase of indentation load, as seen in Figure 4-1, Figure 4-2 and Figure 4-3. To better

illustrate the creep effect, Figure 4-2 is re-plotted by showing the indenter displacement at each holding-time segment (Figure 4-5). The plots show that the indentation displacement increases rapidly at the initial holding time, then stabilizes at longer holding time, an indication that a quasi-steady flow state may have reached in the material. From these creep plots, the indentation creep rates during holding period can be calculated by $\dot{h}_v = \partial h_v / \partial t$ [**33**,**34**]. In this paper, the indentation creep rate, $\dot{h}_v$, was normalized with the indenter unloading rate, $\dot{P}$, where $\dot{P} = \partial P / \partial t$. The normalized creep rate ($\dot{h}_v / \dot{P}$), the third term in Equation (4.4), can be viewed as a "creep factor" during the indentation of polymeric materials. It is seen that a small creep factor would require a long load-hold period and/or a fast indenter unloading rate.

The normalized indentation creep rates ($\dot{h}_v / \dot{P}$) of the present PMR-15 were calculated, based on the results shown in Figure 4-5. Overall, the indentation creep rates, or the creep factors, are higher at the beginnings of the indenter holding period and then decrease with increasing the holding time (Figure 4-6). The creep factor is also affected by the indenter unloading rate ($\dot{P}$). The larger the $\dot{P}$, the smaller the creep effect. For the present highly cross-linked PMR-15 polyimide, the creep factor has become negligibly small at longer holding time. These experimental results are consistent with a recent study by Cheng and Cheng [**31**]. They conducted the finite element simulation on nanoindentation of viscoelastic materials and found that the contact stiffness obtained from the initial unloading response may be affected by the indenter holding history and initial unloading condition. An indenter hold period is necessary to minimize the creep effect occurred at the onset of indenter unloading. The creep effect can also be reduced by using a fast unloading rate.

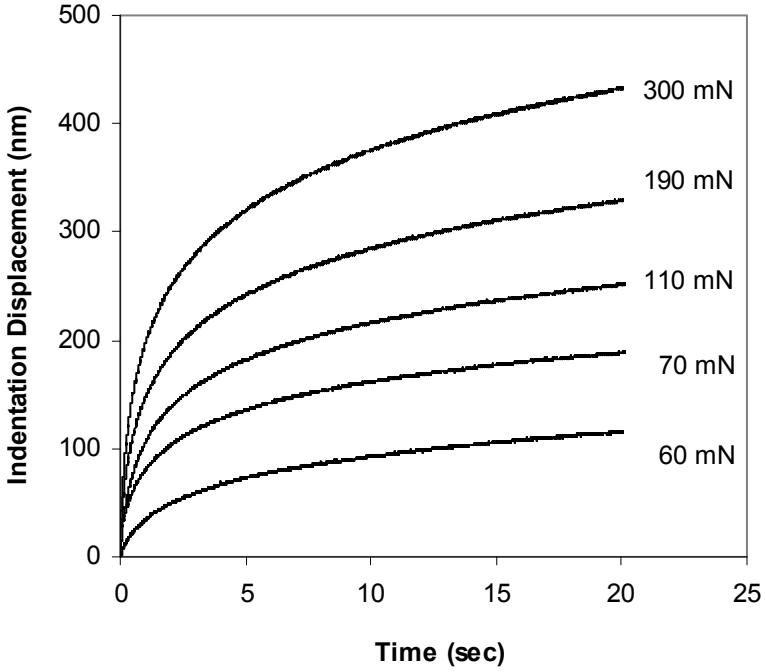

Figure 4-5 Creep response of PMR-15 during hold period. This figure is a re-plot of the holding-time segments in Figure 4-2.

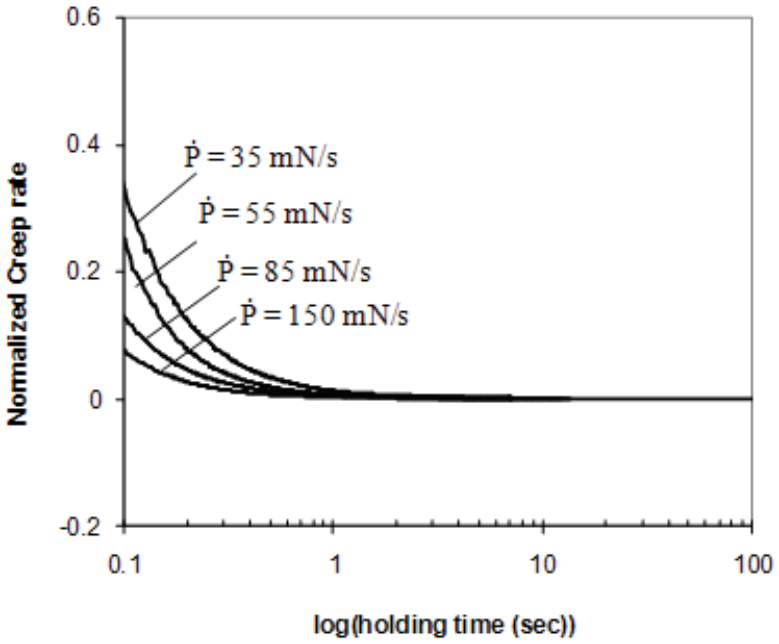

Figure 4-6 Variations of normalized creep rates (creep factors) during nanoindentation of PMR-15 polyimide at ambient temperature.

Various indenter holding times have been used in the present PMR-15 experiments, ranging from 0.1 to 120 s (Figure 4-7). From the initial unloading responses, the elastic contact stiffness, S_e, was calculated as a function of holding time, via Equation (4.3). As seen in Figure 4-9, S_e remains relatively unchanged at longer holding times (as $t > 1$ s). Similar results have been reported by other researchers [**30**,**32**]. For example, Briscoe et al [**30**] has performed the nanoindentation tests on an amorphous polymethylmethacrylate (PMMA) using a holding time up to 300 s and found that the apparent stiffness is stable with increasing holding time. Geng et al [**32**] used a similar indenter to test a low modulus polymer film and showed that the indentation modulus remained unchanged after a 2s holding period. (The creep component during the initial unloading was not subtracted from the apparent stiffness in those papers). Also shown in Figure 4-9 is the variation of the elastic component of the total indenter displacement (h_{max} - h_{creep}), the first term in Equation (4.4). As expected, this term is independent of the holding time. The unloading rate $\dot{P}$ was 250 mN/s.

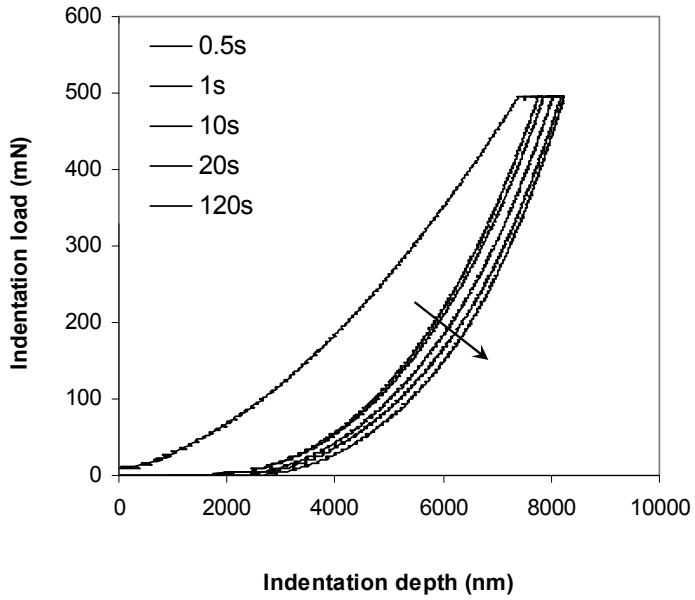

Figure 4-7 Effect of holding time on indentation unloading responses of PMR-15 polyimide. The arrow points to the direction of longer holding time.

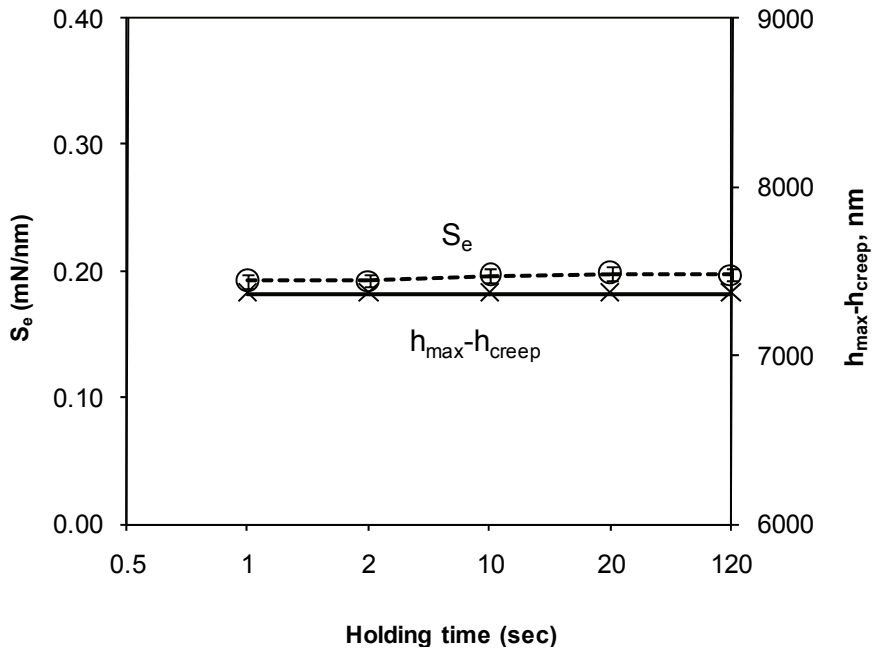

Figure 4-8 Effect of holding time on elastic contact stiffness (S_e) and total elastic deformation ($h_{\max} - h_{creep}$) of PMR-15.

4.4.2 NANOINDENTATION OF PMR-15 AT AMBIENT TEMPERATURE

From the load-depth curves, critical parameters such as h_{max}, h_{creep}, P_{max}, $\dot{h}_v$, $\dot{P}$ and S were obtained. Substituting the information into Equations (4.4)(4.5)(4.6)(4.7), the elastic modulus and hardness of the PMR-15 were computed. Figure 4-10 shows the dependence of the average elastic modulus of PMR-15 on holding time. The modulus is higher initially since the creep effect is dominant at smaller holding time. Then, the modulus converges to a plateau value as the holding time is greater than approximately 1 s. Concerning all other potential effects (including the instrument drift to be discussed in later section), a 2 s holding time is deemed to be sufficient and used in subsequent experiments. The optimal holding time depends upon the material tested. In general, a stiffer polymer requires a shorter holding time.

The mechanical properties obtained from nanoindentation experiments may be affected by the surface quality of the specimen. In the current experiments, the polymer specimens were prepared by grinding papers and polishing compounds, the final polishing compound being alumina with an average particle size of 0.3 μm. The surface profile of

the present PMR-15 specimen has been studied by using a White Light Interferometer (WYKO NT1100). The White Light Interferometer scans the surface of the specimen vertically and generates the surface topography in three-dimensions. By analysing the 3D image, quantitative information about the surface can be calculated. The average roughness of the surface is approximately 170 nm. In addition to the surface imperfectness, the outer layer of the specimen may be strain hardened during sample preparation stage (the surface of the specimen is polished aggressively through various polishing compounds). All these factors can contribute to errors in estimating the true mechanical properties during nanoindentation.

In the present experiments, the indenter was programmed to cyclically load and unload into the specimen under progressively increased load, up to a maximum of 500 mN. This way, the indentation load-depth curves were recorded at various depths, as illustrated earlier in Figure 4-1, Figure 4-2, Figure 4-3, and Figure 4-4. From those curves, the depth-dependent elastic modulus and hardness were computed through Equations (4.4) (4.5)(4.6)(4.7). As seen in Figure 4-11 and Figure 4-12, the modulus and hardness are higher at shallower depths, and then reach plateau values at a depth greater than approximately 500 nm. The average elastic modulus and hardness determined for unaged PMR-15 resin is 4.26 GPa and 0.44 GPa, respectively, which are close with results reported in literatures (obtained by dynamic modulation method) [**35**,**9**].

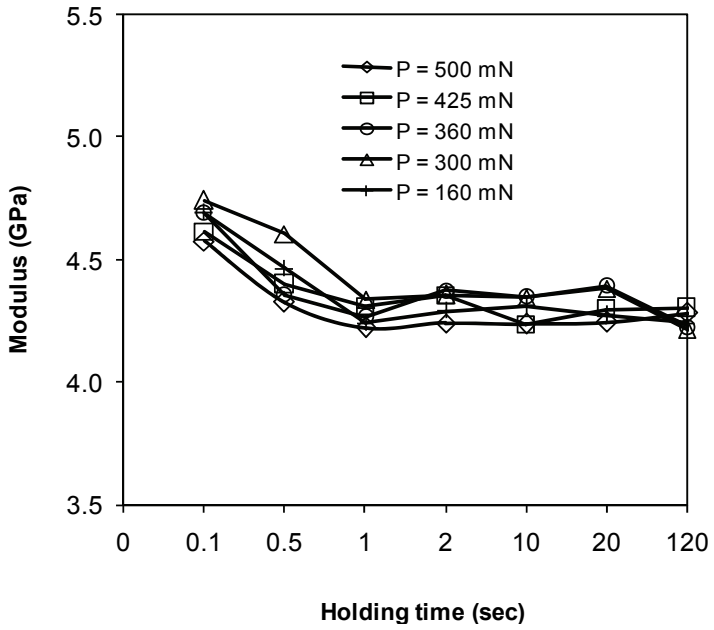

Figure 4-9 Effect of holding time on elastic modulus of PMR-15 polyimide at ambient temperature.

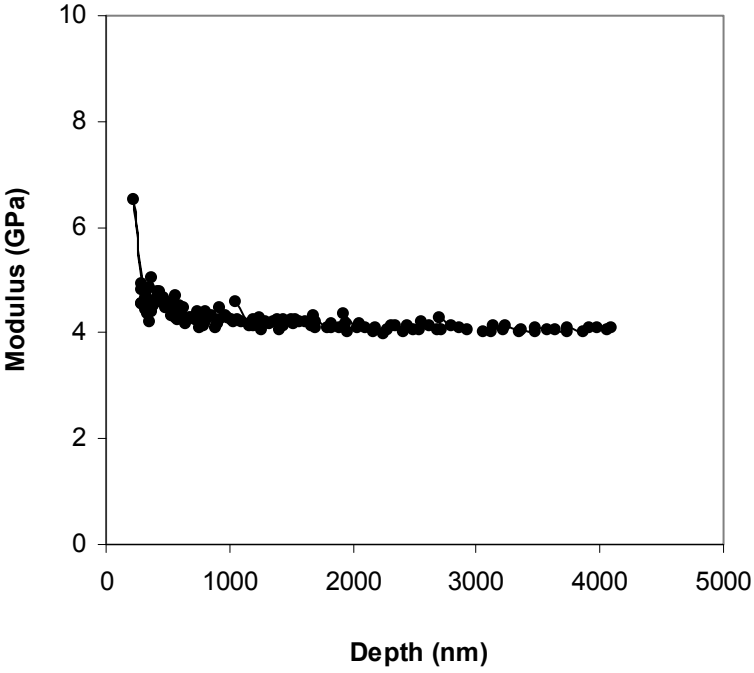

Figure 4-10 Indentation depth dependent elastic modulus of PMR-15 polyimide at ambient temperature.

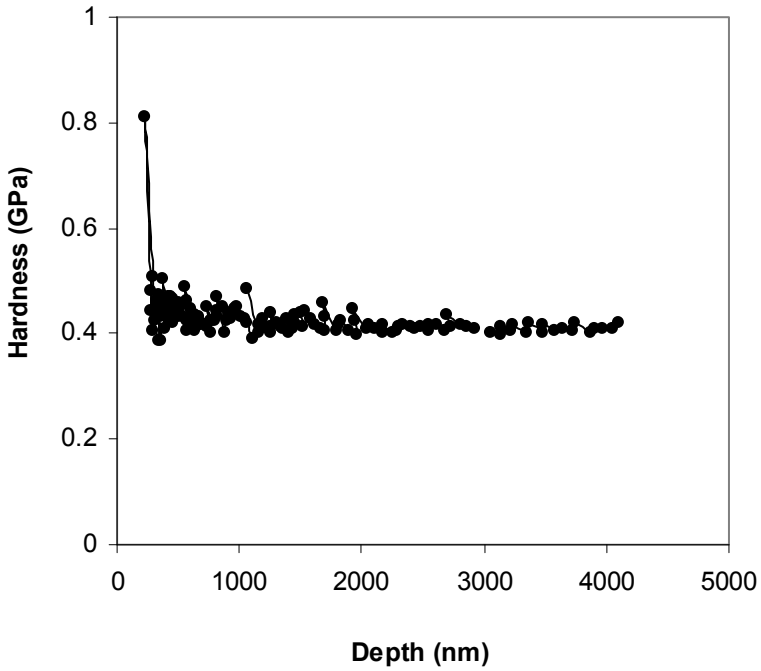

Figure 4-11 Indentation depth dependent hardness of PMR-15 polyimide at ambient temperature.

4.4.3 NANOINDENTATION OF PMR-15 AT ELEVATED TEMPERATURES

Although a substantial body of literature is available on nanoindentation, only a few have dealt with nanoindentation at high temperatures and the studies have been mostly concentrated on standard reference material, i.e., high purity fused silica. Beake and Smith are apparently the first who have reported the high temperature nanoindentation experiments [**27**]. They used a nanoindenter from Micro Materials Ltd (Wrexham, UK) to examine the mechanical properties of fused silica up to 400°C. The results show that the elastic modulus of fused silica increases by a factor of 1.1 as the temperature increases from ambient to 200°C. Schuh et al [**28**] tested fused silica by using a nanoindenter from Hysitron, Inc (Minneapolis, USA) with a custom-built heating-cooling system. It is concluded that the modulus of fused silica increases by about 1% for every 100 K, or by a factor of 1.01 from room temperature to 200°C.

The current high temperature experiments were performed on a MTS Nano Indenter (Oak Ridge, TN) using XP mode. The indenter is equipped with a hot-stage heating system and a thermal-protective shield (to prevent the radiation of heat from hot-stage to indenter

transducer assembly). Prior to testing PMR-15, the fused silica was examined. Figure 4-12 shows the load-depth curves of fused silica tested from 120°C to 240°C. It is observed that there is negligible difference in load-depth responses. Detailed calculations show that the modulus of fused silica increases by a factor of approximately 1.02 as temperature is raised from ambient to 200°C, which is consistent with the finding reported by Schuh et al [**28**], shown previously in Figure 3-13.

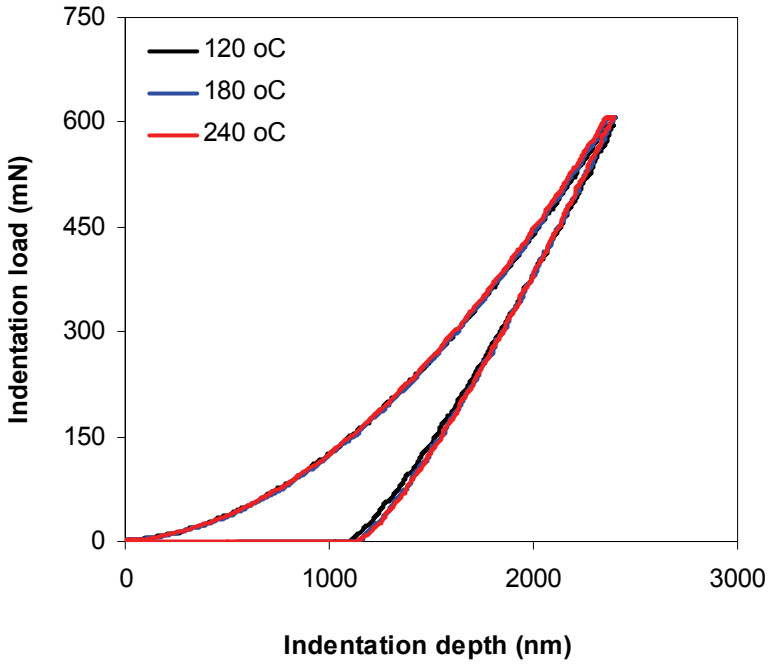

Figure 4-12 Indentation load-depth curves of fused silica at elevated temperatures.

The nanoindentation tests were then performed on PMR-15 polyimide resin at elevated temperatures (50, 75, 100, 150, 200°C). A 2 s holding time derived earlier has been used for all experiments. Different holding times have been investigated at elevated temperatures and results indicate that a 2 s holding period seems to be sufficient for minimizing the creeping effect on initial unloading response (Figure 4-13). Holding the indenter for a longer time at elevated temperature may not be beneficial since it may introduce additional errors due to the presence of thermal drift. In a high temperature nanoindentation experiment, the potential sources of thermal drift may include the thermal expansion of indenter tip, the transient thermal contraction at tip-specimen

interface, and electric drift of the sensing and actuating devices. Over a longer period of holding time, these potential drifts may cause additional movements at the indenter tip and thus affect the indentation response. The drift effect becomes evident on the creep curve of PMR-15 at 200°C as recorded during indenter holding time segment (Figure 4-14). Compared to the smooth creep curve obtained at ambient condition, the creep curve at 200°C is much nosier, showing signs of both expansions/contractions due to various sources of thermal drifts.

Figure 4-15 shows the indentation loading-unloading responses of PMR-15 at elevated temperatures (50 to 200°C). The load-depth curve becomes less stiff as temperature increases. Following the same analysis procedures used in room temperature experiments, the elastic modulus and hardness were computed. A total of 36 measurements were conducted at each temperature on two separate specimens. Measurements obtained at each testing condition are consistent and the amount of error (deviation) is small (Table 4-1, Figure 4-16). This indicates that the current high temperature nanoindentation technique is reliable for quantitative characterizations of local material properties at elevated temperatures.

Finally, the average elastic modulus of unaged PMR-15 resin obtained from nanoindentation tests is plotted as a function of temperature, as shown in Figure 4-17. Also shown in the figure are the temperature-dependent elastic moduli of the same PMR-15 resin obtained from conventional tension and compression tests. The overall trend from nanoindentation test is consistent with those from macroscopic tests. It is noticed that the polymer resin has slightly higher modulus under compressive mode. This is likely a result of the hydrostatic component of the stress field when the specimen is under compression, since the mechanical properties of polymers are known to be pressure dependent [**36**].

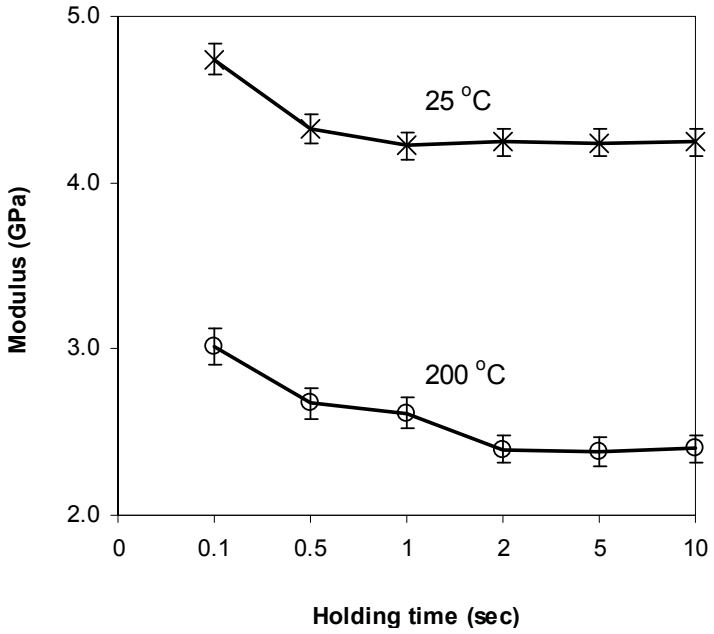

Figure 4-13 Effect of holding time on elastic modulus of PMR-15 polyimide at 200°C.

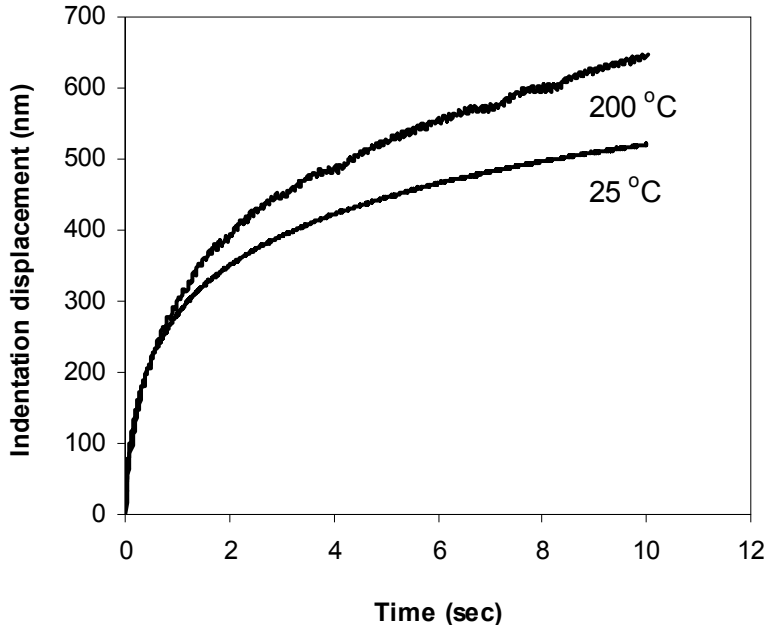

Figure 4-14 Creep responses of PMR-15 during indenter holding segment ($t = 10\,\mathrm{s}$).

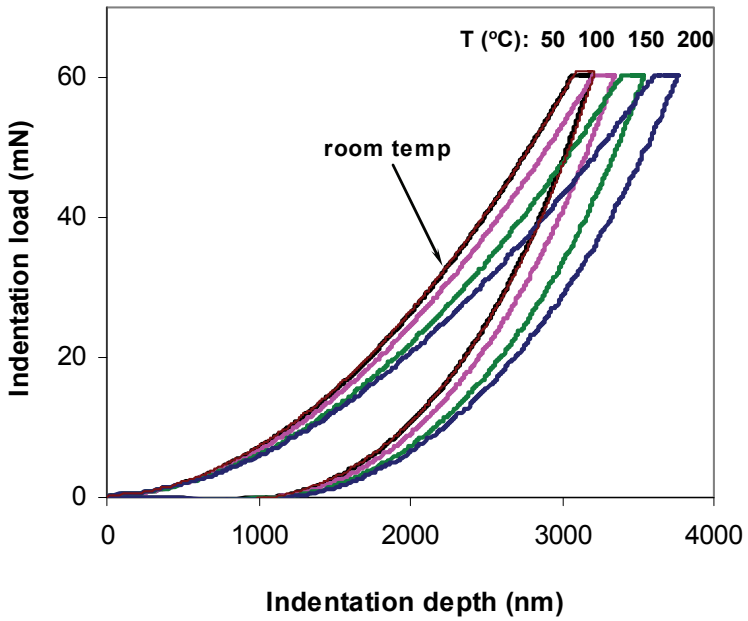

Figure 4-15 Load-depth curves of PMR-15 at elevated temperatures.

Table 4-1 The elastic modulus and hardness of PMR-15 polyimide measured at ambient and elevated temperatures. The statistical values are computed based on a total of 36 measurements conducted at each temperature.

Temperature (°C)	Modulus * (GPa)		Hardness * (GPa)	
	Specimen one	Specimen two	Specimen one	Specimen two
23	4.26 (0.12)	4.28 (0.13)	0.44 (0.04)	0.45 (0.03)
50	4.14 (0.12)	4.16 (0.12)	0.42 (0.02)	0.42 (0.02)
100	3.75 (0.16)	3.74 (0.09)	0.37 (0.02)	0.38 (0.02)
150	3.35 (0.08)	3.46 (0.12)	0.35 (0.01)	0.35 (0.01)
200	2.73 (0.06)	2.75 (0.09)	0.31 (0.01)	0.30 (0.02)

* Numbers in parenthesis are standard deviations

(a)

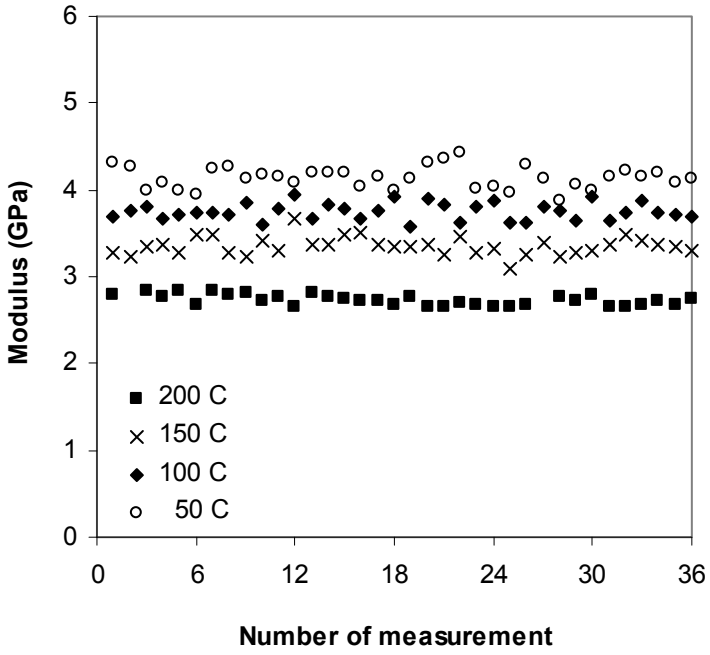

(b)

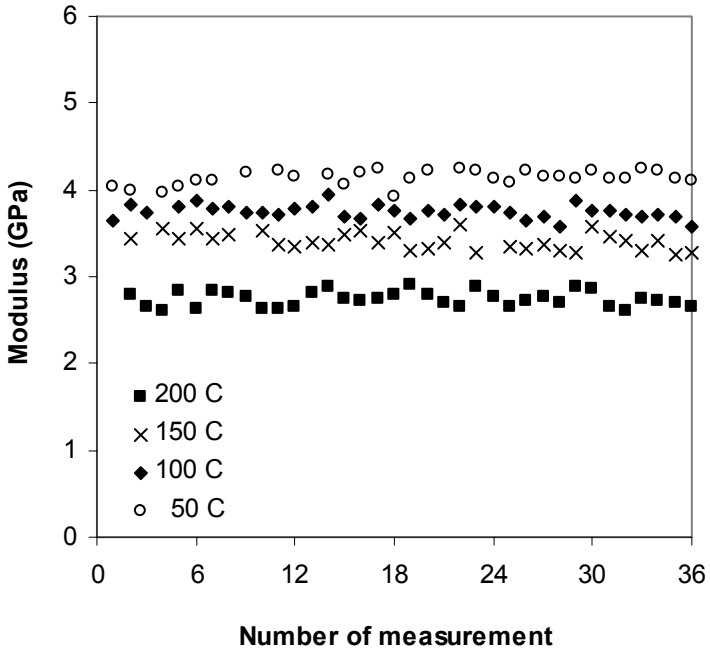

Figure 4-16 Variations of elastic modulus of PMR-15 polyimide as a function of number of measurements from (a) specimen one and (b) specimen two.

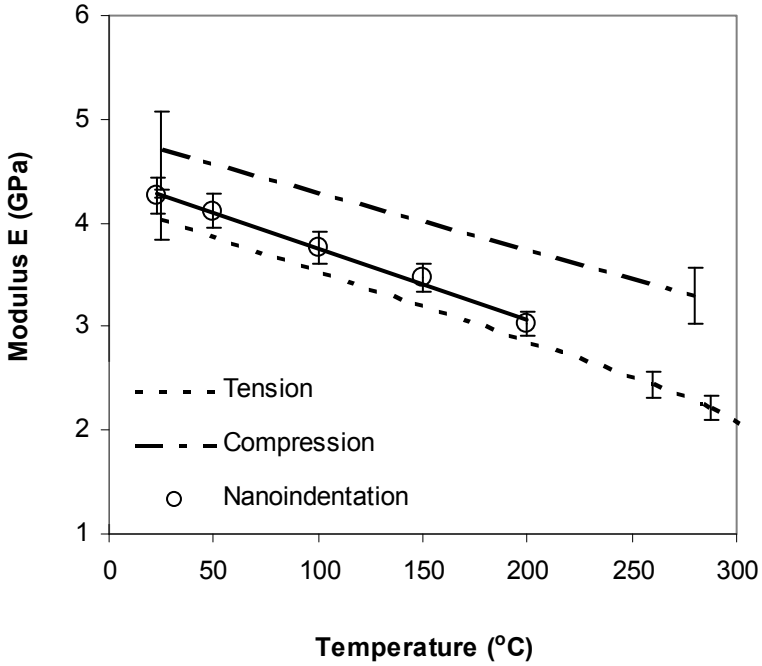

Figure 4-17 Temperature-dependent modulus of PMR-15 obtained from high-temperature nanoindentation. The dashed lines show the Young's modulus obtained from conventional tension and compression tests.

4.5 CONCLUSIONS

The high temperature nanoindentation tests have been performed on unaged PMR-15 polyimide neat resin using a nanoindenter equipped with a hot-stage heating system. The indenter has been programmed to perform the "hold-at-the-peak" experiments using various indenter holding times and unloading rates. Analytical procedures have been modified to take into account the holding time and unloading rate so that the correct contact depth, along with elastic modulus and hardness, can be calculated. The effective holding time was determined for PMR-15 at both ambient and elevated temperatures.

The high temperature mechanical properties of unaged PMR-15 neat resin have been examined with the nanoindenter up to 200°C, and the results follow the same trend as macroscopic test data. Statistical analysis reveals that the variations in nanoindentation measurements performed at elevated temperatures are at a minimum, indicating that this high-temperature nanoindentation technique is reliable for quantitative characterizations of mechanical properties of polymers/composites at elevated temperatures.

CHAPTER FIVE NANOINDENTATION TESTING OF THERMALLY OXIDIZED PMR-15 POLYIMIDE

5.1 INTRODUCTION

This chapter presents the high temperature nanoindentation experiments performed on thermo-oxidatively aged PMR-15 polyimide. A series of PMR-15 resin specimens were isothermally aged at various temperatures, times and pressures. The elastic moduli across the oxidized surface layer were subsequently measured using the nanoindenter. Results show that the average modulus in the oxidized surface layer is notably higher than that in the unoxidized interior, indicating that the oxidized surface layer has limited ductility and thus is susceptible to fracture. Effects of aging environments (time, temperature and pressure) on mechanical properties are also examined. Once passing the initial oxidation stage, the change in modulus become insignificant and less sensitive to aging parameters.

5.2 EXPERIMENTAL

5.2.1 SAMPLE PREPARATION

Rectangular PMR-15 neat resin plaques were fabricated in an autoclave using a steel die mold with Teflon coating and the manufacturer's suggested cure cycle. Subsequent to the plaque being post-cured in air for 16 hr at 316°C, it was cut using a diamond wet-saw with distilled water as a cooling media. The sample was then washed using a common household soap and then rinsed with distilled water for a minimum of 5 min. The specimen was then dried with standard paper towels and placed in a vacuum oven at 105°C for a minimum of 48 hr to remove any moisture within the samples, and stored in a nitrogen purged desiccator until testing. The specimen was isothermally aged at various temperatures (288, 316, and 343°C). The aging time ranged from 1 hr to over 3000 hr. The aging pressures used were ambient pressure, 0.414 MPa, and 0.62 MPa.

Smaller specimens were subsequently dry-sectioned from the aged plaques using a diamond saw with distilled water as a cooling media. The specimen was then potted in Jeffamine 828-D230 epoxy resin that was cured at room temperature for three days. The

surface of the specimen was prepared by grinding papers and polishing compounds, the final polishing compound being alumina with an average particle size of 0.3 μm. These potted cross-sections were used for optical microscopy and nanoindentation measurements.

5.2.2 Optical Examination

The Nikon Microphoto-FXL, Model F84006, in the bright-field mode was used to examine the morphology of the oxidized materials. The intensity of the microscope light was adjusted such that the entire aged sample was well illuminated. Care was exercised to ensure that the potted specimen was flat once the oxidation layer was in view under the microscope. This was done by verifying that the layer is approximately of same thickness on all sides of the specimen. If it was not, the sample might have been cut obliquely or not mounted flat and would need to be reprepared. The edge of the aged specimen was then brought into focus, and the thickness of the oxidative layer and transition region were measured (The definitions of "oxidative layer" and "transition zone" are given later in Results and Discussion section – 5.3.1). A total of 12 measurements were made, three thickness values along each edge of the specimen, and the averages were computed.

5.2.3 Nanoindentation Test

The nanoindentation tests were performed on a Nano Indenter XP (MTS NanoInstruments, Oak Ridge, TN) with a Berkovich diamond tip. The indenter has a nominal tip radius of $r < 20$ nm and an inclined angle of $\theta = 65.3°$. The elastic modulus of the aged specimens were performed by following the "hold-at-the-peak" method, a procedure used for testing viscoelastic materials as discussed in Chapter 4. That is, the indenter was first loaded into the specimen and then held at the maximum load for a certain length of time (2 s) prior to unloading. The purpose of this procedure was to reduce the viscoelastic effect on indentation unloading response so that the correct elastic stiffness could be calculated. The spatial variability in modulus of the PMR-15 was investigated by a "scan-indentation" technique. The scan-indentation is a series of indentation across oxidized surface layer and unoxidized interior. Enough distance was given between indentations to minimize the effect of residual stresses from previous

indentations. Specimens used were aged at 288°C in 0.414 MPa pressurized air for 651 hr and 1518 hr, respectively. On each specimen, the scan was first performed from the oxidized edge towards the unoxidized central region, and then from the central region towards the edge. The test were conducted at ambient and elevated temperatures.

5.3 RESULTS AND DISCUSSION

5.3.1 PHENOMENOLOGY OF THERMAL OXIDIZATION OF PMR-15

The morphologies of isothermally aged PMR-15 specimens were examined with optical microscope (Nikon Microphoto-FXL, Model F84006) using a bright-field light. Figure 5-1 shows an optical micrograph of a PMR-15 neat resin specimen isothermally aged at 316ºC for a period of 215 hr in ambient air; Figure 5-2 shows an optical micrograph of a PMR-15 neat resin specimen isothermally aged at 288ºC for a period of 651 hr in 0.414 MPa pressurized air. These micrographs reveal that there exist three distinct material regions, representing different levels of oxidation. They are: region I - the fully oxidized surface layer, region II - the active reaction zone (where a mix of oxidized and unoxidized polymers exist), and region III - an unoxidized interior. The thickness of the active reaction zone (region II) is rather small and can reduce in thickness as aging temperature increases [**1**,**2**,**3**].

The micrographs reveal that small voids have developed in the oxidized regions, particularly at longer aging time and higher aging pressure Figure 5-2. The presence of voids has been explained by Meador et al [**5**] using the Kirkendall effect. The Kirkendall effect refers to the migration of atoms in a solid at an interface. In the oxidation process, the inward diffusion of oxygen is slower than the outward diffusion of degradation products, therefore, the small voids form. Voids can increase in size and density over time, which act as starter points for microcracks.

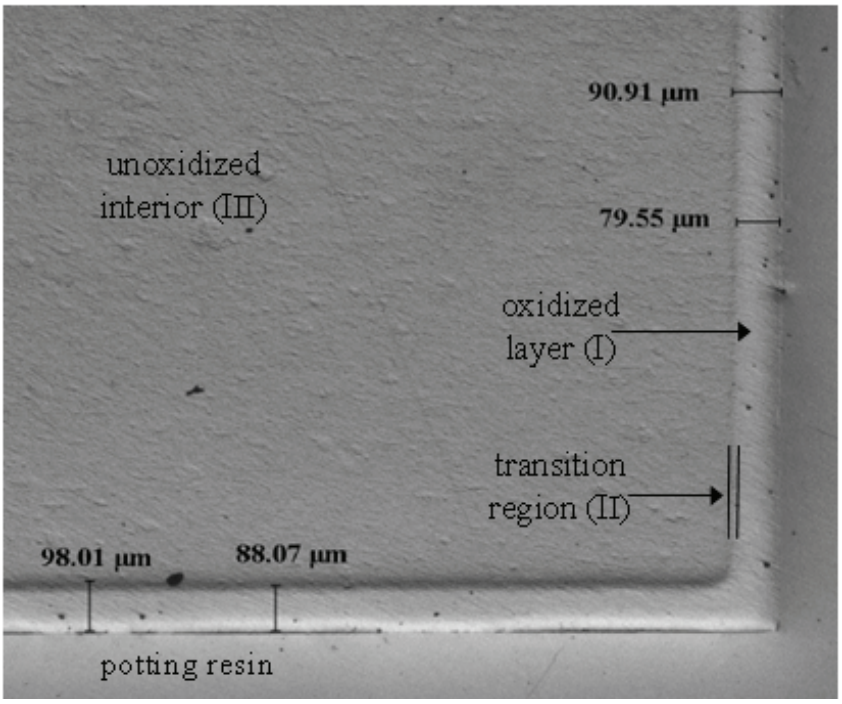

Figure 5-1 Optical micrograph of oxidized PMR-15 polyimide aged at 288ºC for 215 hr in lab air.

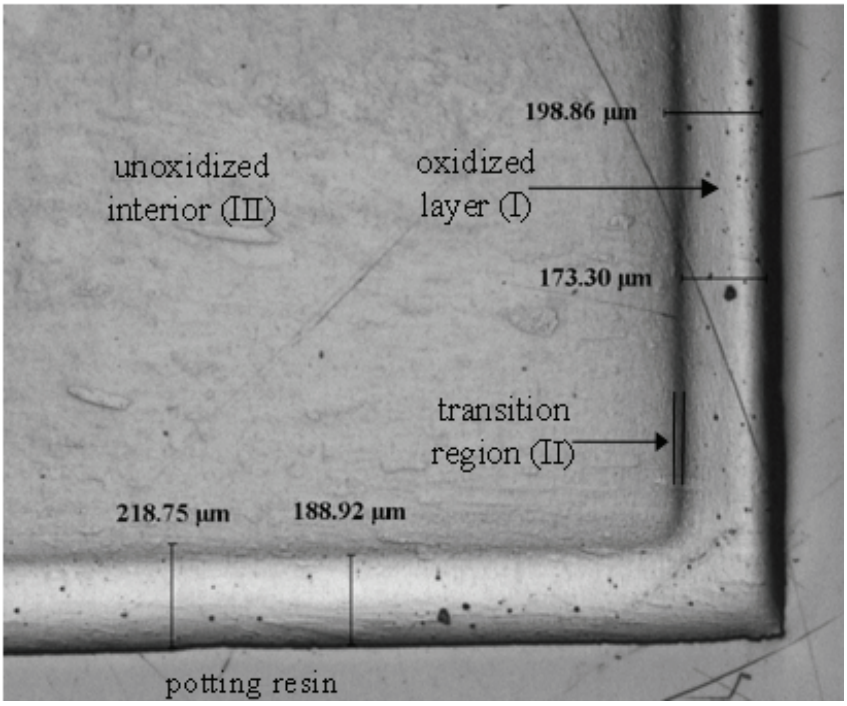

Figure 5-2 Optical micrograph of oxidized PMR-15 polyimide aged at 288ºC for 651 hr in 0.414 MPa pressurized air.

The thickness of the oxidized surface has been found to depend upon the environmental conditions (time, temperature and pressure) [**1**,**2**,**3**]. The effect of aging time on oxidized surface thickness is shown in Figure 5-3 for PMR-15 aged at various temperatures (288, 316, 343 ºC). Within the first hour of thermal aging, an oxidized layer of approximately 10 μm thick is seen to form on the exposed specimen surfaces. Initially, the thickness of this oxidized layer increases rapidly with aging time and then the rate of change starts to decrease. This is because the oxidation growth rate decreases with time over longer aging time periods [**1**].

The oxidization rate is generally accelerated with the increase of aging temperature. Acceleration by temperature occurs by reducing the activation energy of chemical bond rupture in the polymer macromolecule. In the present experiments, the specimens were all aged at relatively high temperatures: 288, 316, 343ºC (typical engine operating temperatures). Within this narrow range of temperatures, the thickness of the oxidized surface is seen to increase, but not substantially (Figure 5-3).

Oxidization growth may also be accelerated by increasing the partial pressure of oxygen within the aging chamber, since the high pressure generally allows the oxygen to diffuse deeper into the interior of the specimens [**1**,**2**,**3**]. In the present experiments, the PMR-15 samples were placed in a steel pressure chamber with a continuous supply of pressurized air (0.414 MPa). The pressure chamber was then put inside an air-circulating oven for elevated temperature aging. Unlike a sealed closed chamber in which the oxygen supply is depleted for long aging times, the present chamber maintains a target pressure while replenishing the air. It is seen that the elevated pressure aging of the PMR-15 resin presumably has a significant effect on the rate of diffusion of oxygen into the specimen, accelerating the oxidation process and allowing the oxygen to diffuse deeper into the interior of the specimens. This results in greater oxidation layer thicknesses than are achievable in ambient air pressure environments (Figure 5-4, Figure 5-2).

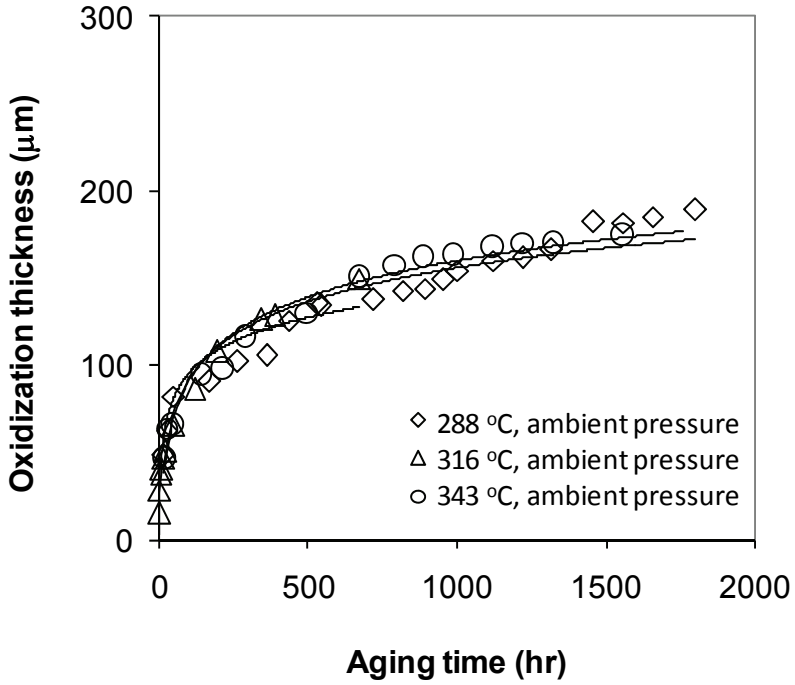

Figure 5-3 Evolution of oxidized surface thickness as a function of aging time. Specimens are isothermally aged at 288, 316, 343ºC.

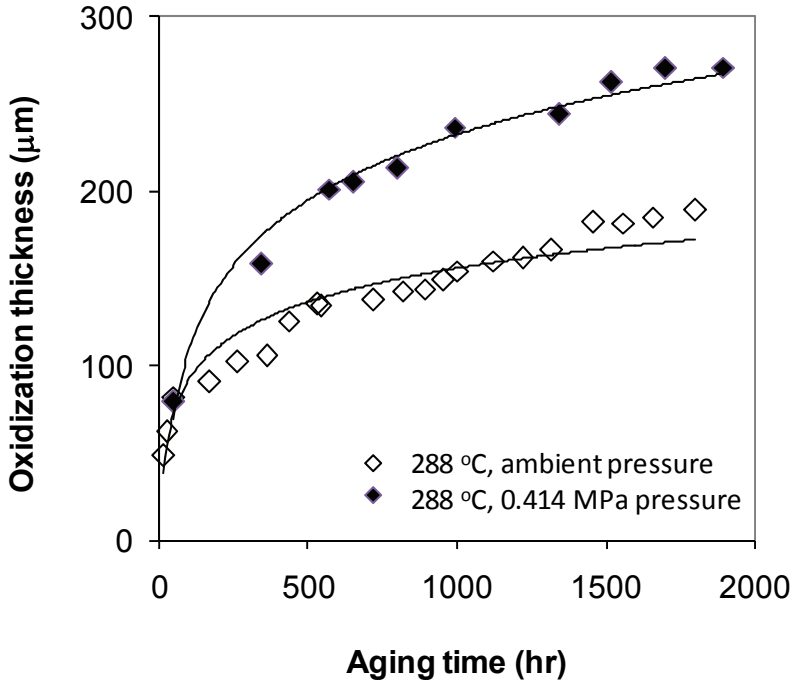

Figure 5-4 Effect of aging pressure on the evolutions of oxidized surface thickness. Specimens are isothermally aged at 288ºC.

5.3.2 Spatial Variability of Modulus of Thermally Oxidized PMR-15

Optical examinations have shown that during oxidation a distinctive oxidized layer and a transition zone form on the exposed specimen. It is thus expected that the specimen's mechanical properties would be inhomogeneous. Nanoindentation tests were performed on cross-sections of oxidized PMR-15 resins (Figure 5-1 and Figure 5-2) to examine the mechanical properties. By indenting exclusively the thin surface layer, the mechanical properties of oxidized material can be precisely measured. The mechanical properties of unoxidized material are obtained by indenting the interior regions of aged specimens.

The spatial variability of modulus of PMR-15 was investigated by a "scan-indentation" technique. The scan-indentation is a series of indentation across oxidized surface layer and unoxidized interior, as illustrated in Figure 5-5 and Figure 5-7, where the dashed lines indicate the "transition zone" measured using optical microscopy. Enough distance was given between indentations to minimize the effect of residual stress from previous indentation. Specimens used were aged at 288ºC in 0.414 MPa pressurized air for 651 hr and 1518 hr, respectively. On each specimen, the scan was first performed from the oxidized edge towards the unoxidized central region (starting from point A to B), and then from the central region towards the edge (starting from point A′ to B′).

The modulus results are shown in Figure 5-6 and Figure 5-8, where the respective transition thickness measured using optical microscopy is denoted by vertical dashed lines. It is seen that the modulus of the oxidized surfaces are notably higher than those of the unoxidized interiors. The results are independent of the choice of initial focus location and therefore of sample surface topography. The higher average modulus in surface layer implies that the oxidized resin has a limited ductility and thus a greater potential for fracture. This is mostly a result of chemical changes occurred during oxidation including chemical bond breakage and outgassing of low-molecular weight species. It is noticed that the modulus within the oxidized layer are approximately the same, indicating that microstructure of this oxidized layer is mostly homogeneous. That has been considered to be the result of a zero-order reaction [**5**,**9**].

Figure 5-9 shows the spatial-dependence modulus of the oxidized PMR-15 specimens tested at elevated temperatures. The moduli of the oxidized surfaces are consistently higher than those of the unoxidized interiors.

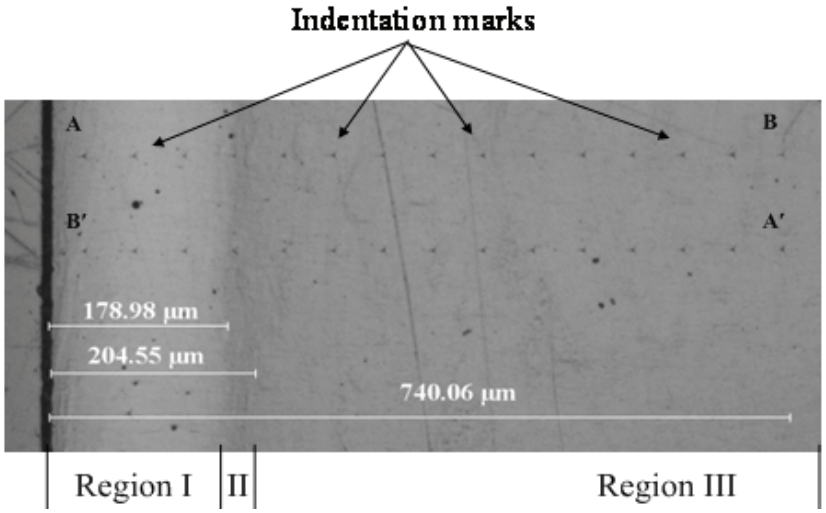

Figure 5-5 Optical micrograph of indented specimen cross-section of oxidized PMR-15 aged at 288ºC for 651 hr in 0.414 MPa pressurized air.

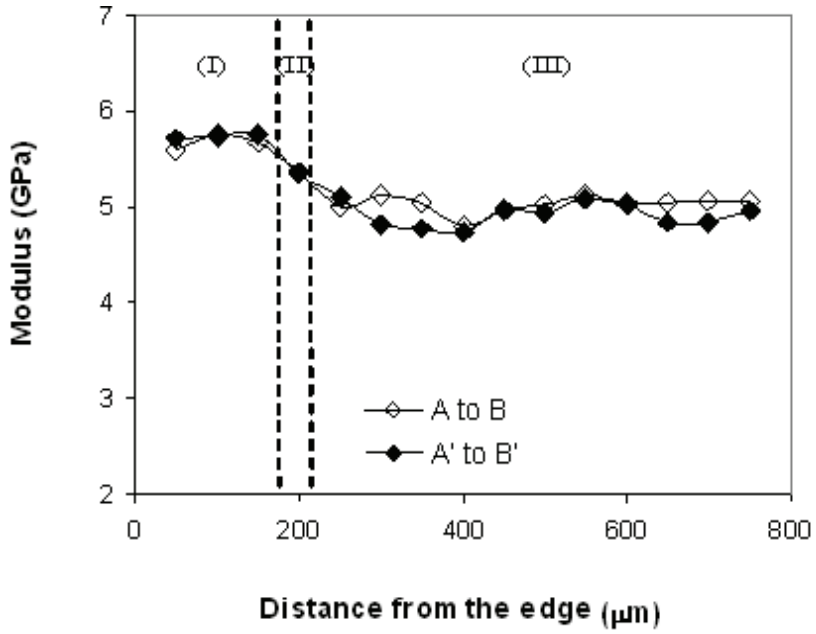

Figure 5-6 Spatial variability of elastic modulus of oxidized PMR-15 aged at 288ºC for 651 hr in 0.414 MPa pressurized air. The dashed lines indicate the "transition zone" measured using optical microscopy.

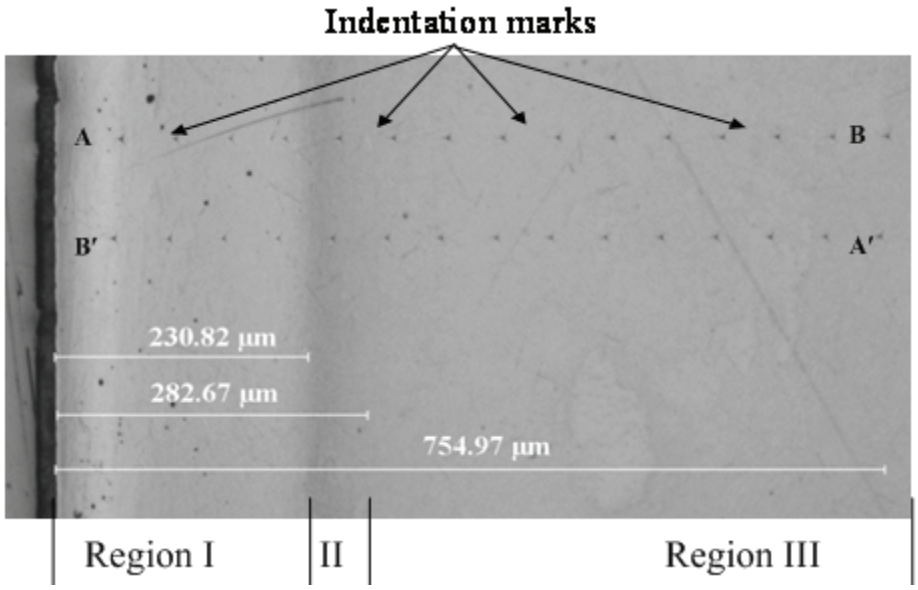

Figure 5-7 Optical micrograph of indented specimen cross-section of oxidized PMR-15 aged at 288ºC for 1518 hr in 0.414 MPa pressurized air.

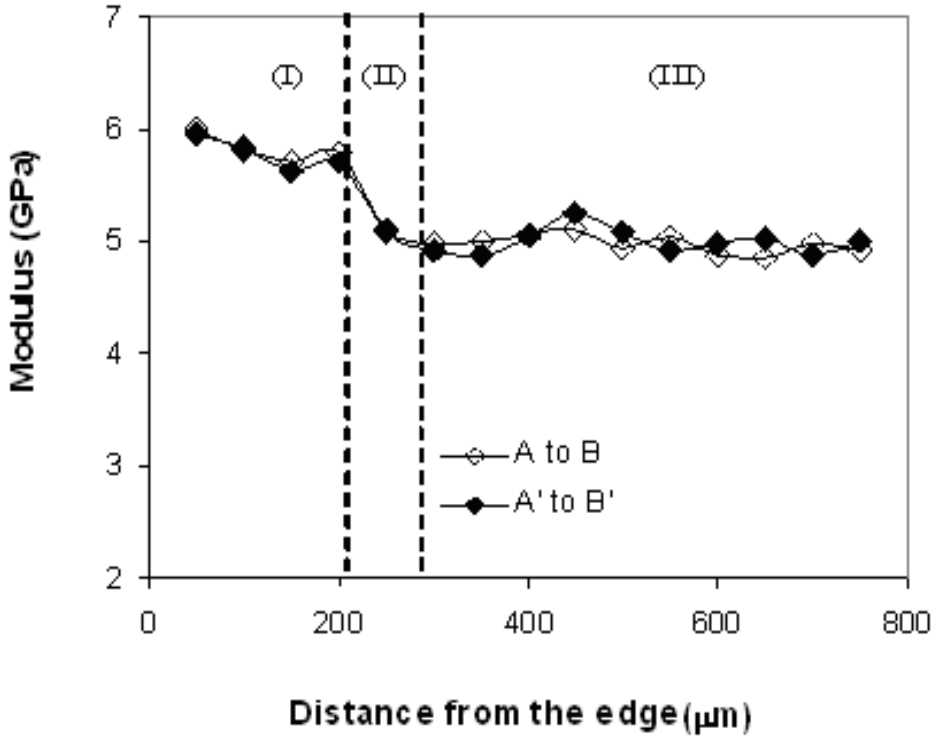

Figure 5-8 Spatial variability of mechanical properties of oxidized PMR-15 aged at 288ºC for 1518 hr in 0.414 MPa pressurized air. The dashed lines indicate the "transition zone" measured using optical microscopy.

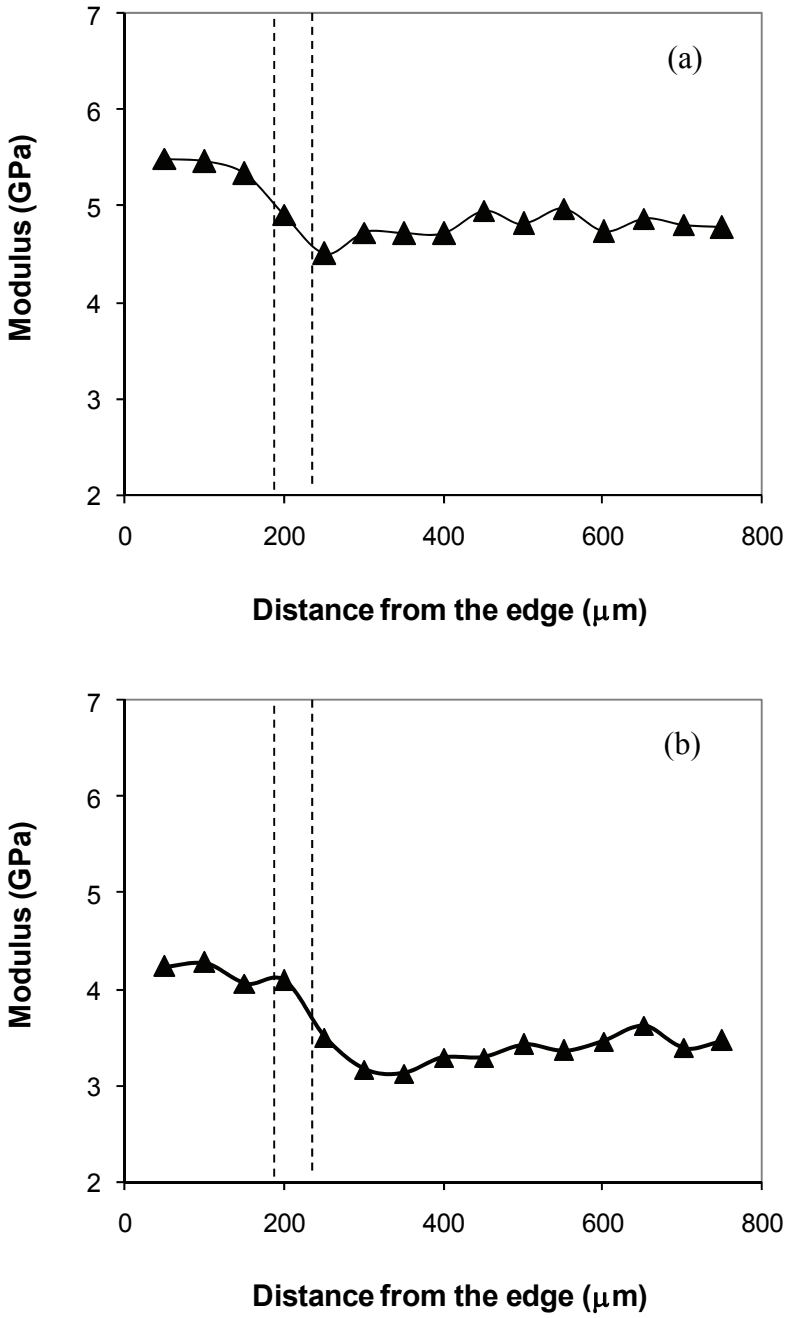

Figure 5-9 Spatial variability of mechanical properties of oxidized PMR-15 resins tested at (a) 50 ^{o}C and (b) 100 ^{o}C. The specimen was aged at 288ºC for 2635 hr in lab air condition. The dashed lines indicate the "transition zone" measured using optical microscopy.

5.3.3 Effects of Environmental Conditions on Mechanical Properties

As discussed in Section 5.3.1, the oxidative profiles of PMR-15 resin specimens are dependent of environmental conditions (time, temperature, and pressure). Longer aging times, higher aging temperatures, and higher aging pressures, can result in a thicker oxidized surface layer, although the most rapid increase generally occurs in the beginning of the oxidation process. The effects of environmental conditions on static mechanical properties have been previously studied using nanoindentation [**9**,**16**]. It is found that once passing the initial aging stage, the elastic modulus in the oxidized region becomes relatively insensitive to variations in aging time, temperature, and pressure.

The effects of environmental variables on rate-dependent properties are investigated here. The nanoindentation tests were performed on specimens with various aging times, temperatures, and pressures. Indentations were performed on the oxidized layer and unoxidized interior, respectively. A total of 15 measurements were made in each region and the average was reported. Figure 5-10 shows the effect of aging time on modulus of PMR-15 aged at 288ºC. The modulus of the oxidized materials increases rapidly in the beginning of aging and then becomes relatively stable for longer aging time periods. This is because over time the oxidation occurs at a much lower rate [**1**,**2**,**3**]. Figure 5-11 compares the modulus of the specimens isothermally aged at 288, 316 and 343ºC. Results show that the moduli of the oxidized materials are consistently higher than those of the unoxidized interiors. Figure 5-12 compares the modulus of the PMR-15 specimens isothermally aged at 288 ºC in a chamber with (a) ambient pressure, (b) 0.414 MPa pressure and (c) 0.62 MPa pressure. Similar to other environmental factors, the aging pressure has accelerated the growth of oxidized surface layer since the rate of diffusion of oxygen into the polymer is increased. But once the polymer is fully oxidized (after the initial oxidation stage), the change in mechanical properties remains at a minimum. Overall, the environmental conditions have the similar effect on modulus as they do on rate-independent property (elastic modulus) as reported earlier [**16**].

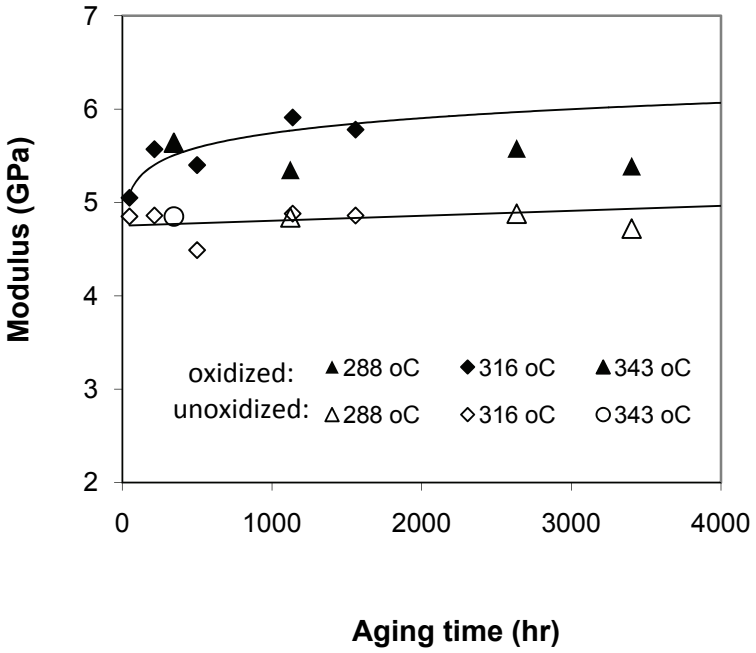

Figure 5-10 Effect of oxidation time on modulus of PMR-15. Specimens used are isothermally aged at 288ºC in lab air.

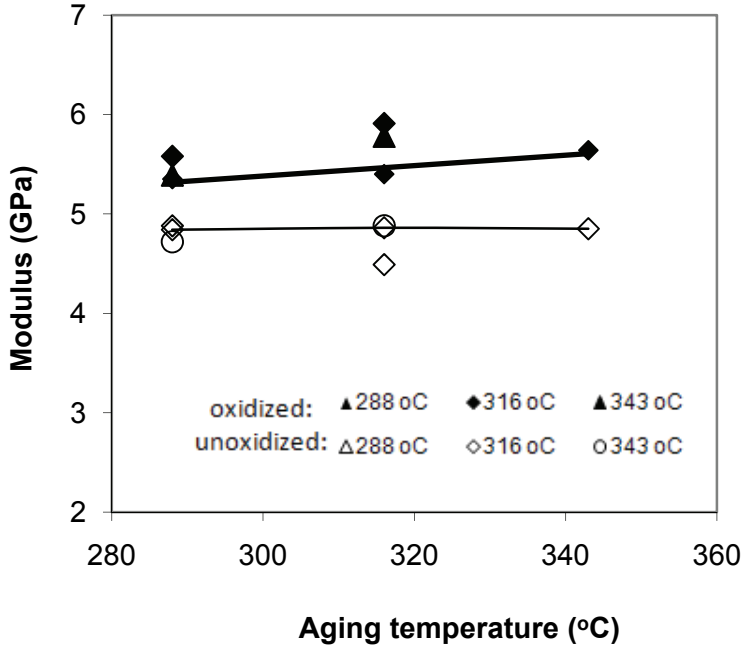

Figure 5-11 Effect of oxidation temperature on modulus of PMR-15. The aging temperatures are 288, 316 and 343ºC.

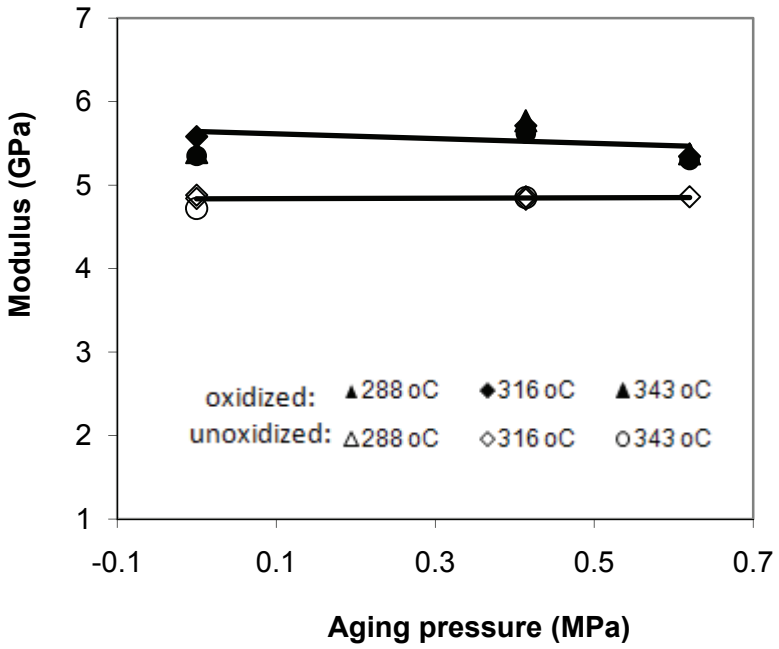

Figure 5-12 Effect of oxidation pressure on modulus of PMR-15. Specimens used are isothermally aged at 288ºC in a chamber with (a) ambient pressure, (b) 0.414 MPa pressure and (c) 0.62 MPa pressure

5.4 CONCLUSIONS

The high-temperature PMR-15 resins have been isothermally aged under a wide range of service environment conditions. The thermo-oxidative behaviour of aged specimens was examined with optical microscopy technique. The oxidation layer thickness increases with increasing aging time initially and then approaches an auto-retardation state.

The spatial variability of modulus has been examined on specimens oxidized at various environmental conditions (time, temperature, and pressure). In all cases, the modulus of oxidized material has been notably higher than that of unoxidized one. Higher modulus in surface layer implies that the oxidized resin exhibits limited ductility and a potential for fracture. The effect of environmental conditions has been examined on various aged samples. Results show that once a material is fully oxidized (passing the initial oxidative period), the modulus is not much influenced by the environmental conditions.

CHAPTER SIX SUMMARY OF CURRENT AND FUTURE WORK

6.1 WORK TO DATE

PMR-15 polyimides have been widely used as matrix materials in fiber-reinforced composites for high temperature aerospace, space and automotive applications. Exposed to elevated temperatures, the polymers undergo thermo-oxidative degradation. Although the physical and chemical properties of aged PMR-15 resin have been extensively studied, the spatial-dependent mechanical properties of this material upon thermo-oxidization requires further assessments. In this thesis, the novel nanoindentation technique has been used to probe the spatial dependent mechanical properties of PMR-15 polymers subjected to thermal oxidation.

Prior to testing the thermally oxidized specimen, the nanoindentation is used to measure the elastic modulus of unaged, homogeneous PMR-15 polymers. The objective is to develop a valid testing and analysis procedure for nanoindentation of polymeric materials. Polymers are viscoelastic materials and thus the properties are time/rate-dependent properties. During nanoindentation testing of PMR-15, the load-depth curves are found to depend upon the indenter holding time and indenter unloading rate. The conventional Oliver-Pharr equation used for analysing the nanoindentation of elastic materials has been modified to take into account of these time dependencies. Various indenter holding times have been investigated and an optimal holding time of 2s is determined for testing the present PMR-15 materials.

The nanoindentation test is then performed on unaged, homogeneous PMR-15 polymers at elevated temperatures (up to 200ºC). Emphasis has been placed on the validation of the high-temperature nanoindentation apparatus. This includes the testing of standard reference material (fused silica) in order to evaluate the thermal stability of the indenter frame. Results indicate that the indenter frame stiffness remains relatively unchanged over the temperature range and that the present apparatus is reliable for performing nanoindentation experiments at elevated temperatures.

The nanoindenter is subsequently used to probe the spatial dependent mechanical properties of thermally oxidized PMR-15 polymers. The oxidization profile of the isothermally aged PMR-15 specimen is first studied using optical microscope. Results show that the oxidized specimen exhibits three distinguished regions: region I - the fully oxidized surface layer, region II - the active reaction zone (where a mix of oxidized and unoxidized polymers exist), and region III - an unoxidized interior. The thickness of the oxidized surface layer is seen to increase with the increase of aging time, although the rapid increase occurs mostly at the beginning of the aging time (~200 hr), and also increases with increased aging pressure.

The spatial variability of elastic modulus of the thermo-oxidized PMR-15 specimen is obtained by "scan-indentation" technique, i.e., the indentation is conducted across the aged specimen. Results indicates that the moduli are generally higher at the oxidized layer than those at the unoxidized interior. This is a result of the physical/chemical degradation of the surface materials. The effect of environmental conditions (aging time, aging temperature, aging pressure) on mechanical properties of PMR-15 are probed with the nanoindenter. Specimens are isothermally aged at various environmental conditions and the nanoindenter is used to probe the properties of materials at oxidized layer and interior region, respectively. Results show that, under all aging conditions, the oxidized materials exhibit consistently higher moduli than the unoxidized ones. Furthermore, the modulus of the oxidized material is seen to increase rapidly initially and then stabilize over time, due to the fact that the rate of oxidation becomes stable over time.

6.2 FUTURE WORKS

The final goal of the project is to predict the damage and life expectancy of polymer matrix composites used for high temperature structural applications through mechanism-based multi-scale modelling. The framework of these analyses has been summarized in the beginning of this thesis (Introduction section, Figure 1-1). The success of the multi-scale life prediction effort relies on the experimental capability of properly characterizing the evolution of mechanical behavior of each constituent (fiber, matrix, interphase) under the aging conditions. The degradation of carbon fiber upon thermal aging is often considered to be negligible and the properties obtained from conventional bulk testing are

acceptable. The present thesis studies the evolution of mechanical behavior of polymer matrix upon thermo-oxidative aging. Future work should include the investigation of evolution of mechanical property degradation of fiber-matrix interphase after thermal oxidation.

The variation of the mechanical behavior across the interphase can be evaluated as a function of the distance to the interface between the matrix and the fiber using nanoindentation. From the measurements, the extent of thermal oxidation across the interphase can be analysed. A relation between the structural change of the oxidized interphase and its mechanical properties then can be established. This will provide the knowledge required for developing the microstructure-based constitutive relation of HTPMCs.

BIBLIOGRAPHY

[1] G. P. Tandon, K. V. Pochiraju, and G. A. Schoeppner, "Modeling of oxidative development in PMR-15 resin," *Polymer Degradation and Stability*, vol. 91, no. 8, pp. 1861-1869, 2006.

[2] K. V. Pochiraju and G. P. Tandon, "Modeling thermo-oxidation layer growth in high temperature resins," *Journal of Engineering Materials and Technology*, vol. 128, no. 1, pp. 107-116, 2006.

[3] G. A. Schoeppner, G. P. Tandon, and K. V. Pochiraju, "Predicting Thermo-Oxidative Degradation and Performance of High Temperature Polymer Matrix Composites," in *Multiscale Modeling and Simulation of Composite Materials and Structures*. Springer, 2007, pp. 359-462.

[4] N. Regnier, J. Berriot, E. Lafontaine, and B. Mortaigne, "Spectromechanical analysis of the structure and oxidation of PMR thermoset thermally-stable resins," *Polymer Degradation and Stability*, vol. 73, no. 3, pp. 485-490, 2001.

[5] M. A. B. Meador, C. E. Lowell, P. J. Cavano, and P. Herrera-Fierro, "On the oxidative degradation of nadic endcapped polyimides: I. Effect of thermocycling on weight loss and crack formation," *High Performance Polymers*, vol. 8, no. 3, pp. 363-379, 1996.

[6] M. A. B. Meador, J. C. Johnston, P. J. Cavano, and A. A. Frimer, "On the oxidative degradation of nadic endcapped polyimides: 2. Evidence for reactions occurring at high temperature," *Macromolecules*, vol. 30, no. 11, pp. 3215-3223, 1997.

[7] M. A. B. Meador, J. C. Johnston, A. A. Frimer, and P. Gilinsky-Sharon, "On the oxidative degradation of nadic endcapped polyimides: 3. Synthesis and characterization of model compounds for end-cap degradation products," *Macromolecules*, vol. 32, no. 17, pp. 5532-5538, 1999.

[8] H. L. McManus and R. A. Cunningham, "Coupled materials and mechanics analyses of durability tests for high temperature polymer matrix composites," 1995.

[9] L. L. Johnson, R. K. Eby, and M. A. B. Meador, "Investigation of oxidation profile in PMR-15 polyimide using atomic force microscope (AFM) ," *Polymer*, vol. 44, no. 1, pp. 187-197, 2003.

[10] G. Odegard and M. Kumosa, "Elastic-plastic and failure properties of a unidirectional carbon/PMR-15 composite at room and elevated temperatures," *Composite Science and Technology*, vol. 60, no. 16, pp. 2979-2988, 2000.

[11] G. A. Schoeppner and D. B. Curliss, "Model-based design for composite materials life management," in *9th AIAA/ISSMO Symposium on Multidisciplinary Analysis and Optimization*, Atlanta, GA, 2002.

[12] J. L. Broeckert, "Effects of Prior Aging at Elevated Temperature in Air and in Argon Environments on Creep Response of PMR-15 Neat Resin at 288°C," Master's Thesis, WPAFB OH, 2007.

[13] C. M. Falcone, "Some Aspects of the Mechanical Response of PMR-15 Neat Resin at 288 °C; Experiment and Modeling," Master's Thesis, WPAFB OH, 2006.

[14] G. W. Robinson, "High temperature Chemical Degradation of PMR-15 Polymer Resins," Master's Thesis, WPAFB OH, 2005.

[15] C. M. Westberry, "Rate Dependence and Short-Term Creep Behavior of PMR-15 Neat Resin at 23 and 288°C," Master's Thesis, WPAFB OH, 2005.

[16] C. A. Back, "Effects of Prior Aging on the Creep Response of Carbon Fiber Reinforced PMR-15 Neat Resin at 288ºC in an Air Environment," Master's Thesis, WPAFB OH, 2007.

[17] S. Putthanarat, G. P. Tandon, and G. A. Schoeppner, "Influence of aging temperature, time, and environment on thermo-oxidaive behavior of PMR-15: nanomechanical characterization," *Journal of Materials Science*, vol. 43, no. 20, pp. 6714-6723, 2008.

[18] W. Xie, W.-P. Pan, and K. C. Chuang, "Thermal characterization of PMR polyimides," *Thermochimica Acta*, vol. 367-368, pp. 143-153, 2001.

[19] K. A. Patekar, "Long term Degradation of Resin for High Temperature Composites," Final Contractor Report NASA CR-2000-209918, 2000.

[20] K. J. Bowles, D. J. Papadopoulos, L. L. Inghram, L. S. McCorkle, and O. V. Klan, "Longtime durability of PMR-15 matrix polymer at 204, 260, 288 and 316 °C," NASA/TM-2001-210602, 2001.

[21] L. C. Tsuji, H. L. McManus, and K. J. Bowles, "Mechanical properties of degraded PMR-15 resin," NASA/TM-1998-208487, 1998.

[22] E. Ripberger, G. P. Tandon, and G. A. Schoeppner, "Characterizing oxidative degradation of PMR-15 resin," in *S.A.M.P.E. 2004 Symposium and Exhibition*, Long Beach, CA, 2004.

[23] W. C. Oliver, R. Hutchings, and J. B. Pethica, "Measurement of Hardness at Indentation Depths as Low as 20 Nanometres," in *Microindentation Techniques in Materials Science and Engineering*. ASTM, 1985.

[24] G. M. Pharr, D. S. Harding, and W. C. Oliver, "Measurement of fracture toughness in thin films and small volumes using nanoindentation methods," in *NATO Advanced Study Institute on Mechanical Properties of Materials Having Ultra-Fine Microstructure*, Porto Novo, Portugal, 1992.

[25] G. M. Pharr, W. C. Oliver, and F. R. Brotzen, "On the generality of the relationship among contact stiffness, contact area, and elastic modulus during indentation," *Journal of Materials Research*, vol. 7, no. 3, pp. 613-617, 1992.

[26] Y. C. Lu and D. M. Shinozaki, "Deep penetration micro-indentation testing of high density polyethylene," *Materials Science and Engineering*, vol. A249, pp. 134-144, 1998.

[27] G. Huang, B. Wang, and H. Lu, "Measurements of viscoelastic functions of polymers in the frequency domain by nanoindentation," *Mechanics of Time-Dependent Materials*, vol. 8, no. 4, pp. 345-364, 2004.

[28] G. M. Odegard, H. M. Herring, and T. S. Gates, "Characterization of viscoelastic properties of polymeric materials through nanoindentation," *Experimental Mechanics*, vol. 45, no. 2, pp. 130-136, 2005.

[29] M. F. Doerner and W. D. Nix, "A method for interpreting the data from depth-sensing indentation instruments," *Journal of Materials Research*, vol. 1, no. 4, pp. 601-609, 1986.

[30] MTS Systems Corporation, "XP User's Manual: TestWorks® 4 Software for Nanoindentation Systems, Ver.#16," D1418XPA-10629, 2002.

[31] W. C. Oliver and G. M. Pharr, "An improved technique for determining hardness and elastic modulus using load and displacement sensing indentation experiments," *Journal of Materials Research*, vol. 7, no. 6, pp. 1564-1583, 1992.

[32] W. C. Oliver and G. M. Pharr, "Measurement of hardness and elastic modulus by instrumented indentation: Advances in understanding and refinements to methodology," *Journal of Materials Research*, vol. 19, no. 1, pp. 3-20, 2004.

[33] MTS Systems Corporation, "Minus K Table Setup for the Nano Indenter® XP," Supplemental Reference Manual, 2003.

[34] MTS Systems Corporation, "User Instruction: Addendum to the Nano Indenter® XP User's Manuals for the Localized High Temperature Stage," D3409-XPM-12870-0, 2006.

[35] B. D. Beake and J. F. Smith, "High-temperature nanoindentation testing of fused silica and other materials," *Philosophy Magazine*, vol. A82, no. 10, pp. 2179-2186, 2002.

[36] C. A. Schuh, C. E. Packard, and A. C. Lund, "Nanoindentation and contact-mode imaging at high temperatures," *Journal of Materials Research*, vol. 21, no. 3, pp. 725-736, 2006.

[37] A. H. W. Ngan and B. Tang, "Viscoelastic effects during unloading in depth-sensing indentation," *Journal of Materials Research*, vol. 17, no. 10, pp. 2604-2610, 2002.

[38] B. J. Briscoe, L. Fiori, and E. Pelillo, "Nano-indentation of polymeric surfaces," *Journal of Physics, D: Applied Physics*, vol. 31, pp. 2395-2405, 1998.

[39] Y. T. Cheng and C. M. Cheng, "Relationships between initial unloading slope, contact depth, and mechanical properties for conical indentation in linear viscoelastic solids," *Journal of Materials Research*, vol. 20, no. 4, pp. 1046-1052, 2005.

[40] K. Geng, F. Yang, and E. A. Grulke, "Nanoindentation of submicron polymeric coating system," *Materials Science and Engineering: A*, vol. 479, no. 1-2, pp. 157-163, 2008.

[41] Y. C. Lu, D. C. Jones, G. P. Tandon, S. Putthanarat, and G. A. Schoeppner, "High Temperature Nanoindentation of PMR-15 Polyimide," *Experimental Mechanics*, in press.

[42] M. J. Mayo, R. W. Siegel, Y. X. Liao, and W. D. Nix, "Nanoindentation of nanocrystalline ZnO," *Journal of Materials Research*, vol. 7, no. 4, pp. 973-979, 1992.

[43] Y. T. Cheng and C. M. Cheng, "Scaling relationships in indentation of power-law creep solids using self-similar indenters," *Philosophical Magazine Letters*, vol. 81, no. 1, pp. 9-16, 2001.

[44] S. Putthanarat, G. P. Tandon, and G. A. Schoeppner, "Influence of polishing time on thermal-oxidation characterization of isothermoally aged PMR-15 resin," *Polymer Degradation and Stability*, vol. 92, no. 11, pp. 2110-2120, 2007.

[45] R. J. Young and P. A. Lovell, *Introduction to Polymers*, 2nd ed. New York: CRC Press, 1991.

VITA

David Christopher Jones

Born on the 23rd of December in the year 1976 in Murray, Kentucky.

Education

Currently working towards a Master's Degree in Mechanical Engineering at the University of Kentucky.

Received Bachelor's Degree in Mechanical Engineering with a Minor in Mathematics from the University of Kentucky College of Engineering in May of 2007.

Received an Associate's degree in Science from West Kentucky Community and Technical College in August of 2002.

Work Experience

Mechanical Engineer - 06/2008-Present

- Kentucky Space Enterprise
- Lexington, Kentucky

Graduate Research Assistant – 06/2007–Present

- University of Kentucky – College of Engineering
- Lexington, Kentucky
- Air Force Research Laboratory – Materials and Manufacturing Directorate
- Wright Patterson Air Force Base, Ohio

Thermal Engineer - 05/2005-07/2006

- Los Alamos National Laboratory
- Los Alamos, New Mexico

Computer/Mechanical/Chemical Lab Assistant - 07/2002-05/2005

- University of Kentucky – College of Engineering
- Paducah, Kentucky

Publications / Presentations

Lu, Y.C., Jones, D.C., Tandon, G. P., Putthanarat, S., Schoeppner, G. A., "Elastic and Viscoelastic Characterizations of Thermo-oxidized Polymer Resin using Nanoindentation", Journal of Time-Dependent Materials, under review .

Lu, Y.C., Jones, D.C., Tandon, G. P., Putthanarat, S., Schoeppner, G. A., "High Temperature Nanoindentation of PMR-15 Polyimide," Experimental Mechanics, in press.

Rawashdeh, S.A., Jones, D.C., Erb, D.M., Karam, A.K., and Lumpp, J.E., "Aerodynamic Attitude Stabilization for a Ram-Facing CubeSat" AAS 32nd Annual Guidance and Control Conference, Breckenridge, CO, 01/09.

Jones, D.C., et al., "Kentucky Space Facilities for Satellite Development, Testing, and Operation," Technical Poster presented at 2009 Annual Southeast Region Space Grant Meeting, San Juan, Puerto Rico, 01/09.

Jones, D.C., Erb, D.M., Karam, A.K., Tabler, B.B., "Development and Results of Low-Pressure Thermal Soaks for KySat-1," Presented at Space Systems Laboratory Seminar Series, University of Kentucky, Lexington, KY, 11/08.

Lu, Y.C., Jones, D.C., Tandon, G. P., Putthanarat, S., Schoeppner, G. A., "Measurements of Elastic and Viscoelastic Properties of Polymer Matrix Composites Through High Temperature Nanoindentation," Proceedings of the 4th International Conference on Composites Testing and Model Identification, Dayton, OH, 11/08.

Jones, D.C., Lu, Y.C., Schoeppner, G.A., Tandon, G.P., Putthanarat, S., "High Temperature Nanoindentation of PMR-15 Polyimide," IMECE2008-68419; Presented at Proceedings of IMECE2008, 2008 ASME International Mechanical Engineering Congress and Exposition, Boston, MA, 11/08.

Jones, D.C., "Nanomechanical Characterization of Thermo-oxidative PMR-15 Polyimide Resin," Presented at 174th Technical Meeting of the Rubber Division, Louisville, KY , 10/08.

Lu, Y.C., Shinozaki, D.M. and Jones, D.C., "Temperature-Dependent Viscoelastic Properties of Polymers Investigated Through Nanoscale Dynamic Mechanical Analysis," Presented at Symposium on Emerging Methods to Understanding Mechanical Behavior, 137th TMS Meeting, New Orleans, LA, 03/08.

Leifer, J., Jones, D.C., and Cook, A.M., "Gravity-Induced Wrinkling in Sub-Scale, Singly-Curved Parabolic Gossamer Membrane," Paper 2007-1819; Proceedings of the 48th AIAA.ASME/ASCE/AHS/ASC Conference on Structures, Structural Dynamics and Materials: Gossamer Structures Forum, Honolulu, HI, 04/07.

Jones, D.C and Bernardin, J.D., "Thermal Modeling and Experimental Verification of the Interstellar Boundary Explorer's High Energy Neutral Atom Imaging Instrument (IBEX-Hi)," Proceedings to the AIAA Infotech@Aerospace 2007 Conference and Exhibit, Rohnert Park, CA 05/07.

Jones, D.C., Bernardin, J.D., "Computational Modeling and Verification of the Interstellar Boundary Explorer's High Energy Instrumentation Payload (IBEX-Hi)," Presented at 2006 Spacecraft Thermal Control Workshop, Aerospace Corporation, El Segundo, CA 02/06.

Jones, D.C., Cook, A.M., Leifer, J., Lopez, B.C., "Effect of Gravity on Ripple Amplitude Measurement in Sub-Scale, Singly-Curved Parabolic Membrane," Presented at the 2005 Kentucky Space Grant Consortium Conference, Lexington, KY 05/05.

Leifer, J., Jones, D.C., Cook, A.M., Thompson, C., Wainscott, B., "Non-contact Measurement of Gravity-Induced Wrinkling in Scale Model of Parabolic JPL Precipitation Radar," Presented to members of Structure and Materials Technology Group, Jet Propulsion Laboratories, Pasadena, CA, 03/05.

Jones, D.C., and Cook, A.M., "Tension-Induced Rippling of Singly-Curved Parabolic Gossamer Membranes in Zero- and One-g Using Photogrammetry," Technical Poster presented at the 2005 Posters at the Capitol, Frankfort, KY 02/05 and 2005 ASME Regional Student Conference (Region VI), University of Illinois, Champaign-Urbana, IL, 03/05.

Jones, D.C., and Cook, A.M., "Static Analysis of Tensioned, Gossamer Membrane Structures Using Photogrammetry in Microgravity," Presented at the 2004 Kentucky Space Grant Consortium Conference, Lexington, KY 05/04.

Meyer, C.G., Leifer, J., Lopez, B.C., Jones, D.C., and Caddell, B., "Zero- and One-g Comparison of Ripple Amplitude in Single-Curved Parabolic Membranes using Photogrammetry," Proceedings of the 45th AIAA/ASME/ASCE/AHS/ASC Conference on Structures, Structural Dynamics and Materials: Gossamer Structures Forum, Palm Springs, CA 04/04. Also published in AIAA Journal of Spacecraft and Rockets, Vol. 42, Issue 6, 11/05.

Jones, D.C., and Cook, A.M., "Tension-Induced Rippling of Singly-Curved Parabolic Gossamer Membranes in Zero- and One-g using Photogrammetry," Presented at the 2004 AIAA Regional Student Conference (Region II), Purdue University, West Lafayette, IN 04/04.